1 **Phylogenetic Signal in Shell Morphology of the Chemosymbiotic Lucinidae (Bivalvia)**

2

3 Authors: Brooke L. Long-Fox[1,2*], Laurie C. Anderson[3], Shen Jean Lim[4], Barbara J. Campbell[5],

4 Broc S. Kokesh[6], Audrey T. Paterson[7], and Annette S. Engel[7]

5

6 [1]*Department of Chemistry, Biology, and Health Sciences, South Dakota School of Mines and*

7 *Technology, Rapid City, South Dakota, USA;*

8 [2]*Phoenix Bioinformatics, Newark, California, USA;*

9 [3]*Office of Research Affairs, South Dakota School of Mines and Technology, Rapid City, South*

10 *Dakota, USA;*

11 [4]*College of Marine Science, University of South Florida, St Petersburg, FL, USA;*

12 [5]*Department of Biological Sciences, Clemson University, Clemson, South Carolina, USA;*

13 [6]*Department of Integrative Biology, University of California– Berkeley, Berkeley, California,*

14 *USA;*

15 [7]*Department of Earth and Planetary Sciences, University of Tennessee–Knoxville, Knoxville,*

16 *Tennessee, USA.*

17

18 *Correspondence to be sent to Brooke Long-Fox: *Department of Chemistry, Biology, and Health*

19 *Sciences, South Dakota School of Mines and Technology, Rapid City, South Dakota, USA.*

20 *Email: Brooke.Long-Fox@sdsmt.edu*

21

22 **Keywords**: morphology, geometric morphometrics, phylogenetics signal, bivalves

23

Abstract

24   Lucinidae are the most specious family of extant chemosymbiotic bivalves and occupy a wide

25   range of habitats worldwide. All extant lucinids examined to date house chemosynthetic

26   endosymbionts within their gill tissues. Fossil evidence suggests a Silurian origin for the family,

27   with chemosymbiotic associations dating back to at least the Late Jurassic. Previous systematics

28   work indicates that shell characters contain limited phylogenetic signal, and when they do carry

29   phylogenetic signal, it is typically at more derived, genus-level positions. Instead of using

30   categorical states for shell characters, which are ubiquitous in morphological phylogenetics, this

31   study uses landmark-based geometric morphometrics as a quantitative approach to capture

32   morphological variation in shell shape. To test for phylogenetic signal in morphology using the

33   multivariate version of the K statistic (K_{mult}), we analyzed 627 specimens from eight lucinid

34   species. Bayesian phylogenetic analyses were performed on a subset of 62 specimens using four

35   sequenced genes: the nuclear ribosomal genes 18S rRNA and 28S rRNA, and the mitochondrial

36   genes cytochrome *b* (cyt *b*) and cytochrome oxidase I (COI). This study presents the first COI

37   phylogenetic tree for lucinids. Shell shape exhibited a strong phylogenetic signal ($K_{mult} = 0.98$),

38   that was visualized through phylomorphospace analysis (PA), phylogenetically aligned

39   component analysis (PACA), and phylogenetic principal component analysis (Phy-PCA).

40   Although phylogenetic signal was present throughout the entire landmark configuration, thin-

41   Plate Spines (TPS) of mean shell shape illustrated that the inhalant channel shape had the

42   greatest variation among species. Therefore, the phylogenetic signal could not be contributed to

43   any single shell feature or shape.

Introduction

45

46   Lucinidae are a chemosymbiotic marine bivalve family found in habitats ranging from

47   shallow water to bathyal depths (Glover and Taylor 2007; Mikkelsen and Bieler 2008; Taylor et

48   al. 2014). Lucinids occupy a range of latitudes (60°N to 55°S) and habitats, including coral reefs,

49   seagrass beds, mangrove forests, areas of high organic input (such as sewage outflows), oxygen

50   minimum zones, hydrocarbon seeps, mud volcanoes, and hydrothermal vents (Taylor and Glover

51   2010; Taylor et al. 2014). Lucinid associations with chemosymbiotic bacteria are presumed to be

52   ancient, dating to at least the Late Jurassic based on fossils associations of *Beauvoisina* with

53   ancient hydrocarbon seep deposits (Gaillard et al. 1992; Kiel et al. 2010; Stanley 2014; Taylor et

54   al. 2014). However, some fossil evidence suggests that chemosymbiosis in lucinids may extend

55   to the Silurian. The Silurian lucinid *Ilionia prisca* had a life position similar to modern lucinids

56   (i.e., anterior-posterior axis parallel to the sediment-water interface), lived at a depth around 20

57   cm below the sediment-water interface, and exhibited a morphology convergent with the extant

58   *Eomiltha voorhoevei* (Liljedahl 1992; Taylor and Glover 2000).

59   In the shallow marine realm, infaunal lucinid bivalves most commonly inhabit the

60   interface of oxic-anoxic sediment where there is access to high levels of both molecular oxygen

61   (O_2) and hydrogen sulfide (H_2S) (Stanley 1970; Distel and Felbeck 1988; Taylor and Glover

62   2010). Lucinids use their foot to create a mucus-lined anterior inhalant tube to access oxygenated

63   seawater, as well as to tunnel into anoxic sediment to 'mine' sulfide from porewater for

64   oxidation of reduced sulfur compounds, the primary bioenergetic pathway used by the

65   chemosynthetic bacteria associated with lucinids. Lucinids possess anatomical features indicative

66   of symbiont dependence (Fiala-Médioni and Felbeck 1990; Taylor and Glover 2000, 2006), such

67   as an inhalant channel, which is thought to provide additional feeding and respiratory surfaces

68 (Allen 1958; Taylor and Glover 2000). In life, some lucinid species possess an inhalant channel,

69 an area thickened by blood spaces or can consist of complex folds that form the mantle gills

70 (Taylor and Glover 2006). Evidence of the inhalant channel is preserved on the shell interior as

71 the detachment of the pallial line from the elongated anterior adductor muscle scar (Taylor and

72 Glover 2000, 2006).

73   Morphology has played a major role in shaping the classification and evolutionary

74 relationships not only among lucinids but also in other organisms. Phylogenetic relationships

75 among lucinids are complex, as morphology-based taxonomic placement in phylogenies (Chavan

76 1969; Bretsky 1970, 1976) are incongruent with molecular gene-based phylogenies, which has

77 been attributed to homoplasy (Williams et al. 2004; Taylor and Glover 2006; Taylor et al. 2011,

78 2016). Nonetheless, taxonomic classifications based on shell morphology corroborate molecular

79 data and molecular-based phylogenies demonstrate that shell and other anatomical features in

80 closely related taxa are similar (Taylor and Glover 2006; Taylor et al. 2011, 2016). For example,

81 a study of lucinids from the Western Atlantic combined morphological data derived from

82 Bretsky (1970, 1976) with published 18S rRNA data to produce a tree topology like published

83 phylogenies from molecular data only (Christie et al. 2016; Christie 2017). As such, shell

84 features, such as ornamentation or hinge characters, have a potential phylogenetic signal and

85 could be applicable to reconstructing the fossil record (Taylor and Glover 2006; Taylor et al.

86 2011, 2016). This potential was tested in Long-Fox (2022), as morphological shell characters

87 were revealed to produce congruent, albeit poorly resolved, trees compared to those produced

88 using molecular data, indicating that shell characters can be informative in reconstructing lucinid

89 phylogenies. Unfortunately, these congruent clades did not have one or a suite of shell character

90 states that were diagnostic. This limitation was probably due to a restricted number of taxa with

91   available molecular data compared to many more taxa that could be used to investigate shell

92   morphology.

93   In this study, we quantitatively analyzed eight lucinid species by combining molecular

94   gene-based phylogenies with a quantitative morphological approach using landmark-based

95   geometric morphometrics. Combining these approaches provides offers a more effective means

96   of reconstructing evolutionary changes in organismal shape, revealing convergent evolution,

97   assessing morphological diversification within clades, and evaluating how environmental factors

98   influence shape (Sidlauskas 2008; Klingenberg 2010; Stayton 2015; Hopkins 2016). Here, we

99   test for phylogenetic signal in shell morphology to better understand evolutionary relationships

100   within the Lucinidae over geologic time, an analysis not previously applied in such detail to

101   lucinids. This approach offers new insights into the evolutionary and ecological processes

102   shaping this diverse family of chemosymbiotic bivalves. First, we perform Bayesian

103   phylogenetic analyses on newly generated molecular sequences for nuclear ribosomal 18S rRNA

104   and 28S rRNA genes and the mitochondrial cytochrome *b* (cyt *b*) and cytochrome oxidase I

105   (COI) genes. Second, we replace traditional categorical morphological character states with

106   landmark-based geometric morphometrics to assess phylogenetic signal. Finally, test for

107   phylogenetic signal with the multivariate K-statistic (K_{mult}) (Blomberg et al. 2003; Adams 2014)

108   and visualize patterns of continuous morphological variation with three ordination techniques.

                                    Materials & Methods

110   Sampling

111   Eight lucinid species, totaling 627 individuals, were collected from eight Floridian and

112   Bahamian localities (Table 1; Figure 1). Specimens from this project were collected through

113   Florida Fish and Wildlife Conservation Commission (SAL-14-1599-SR) and a Bahamas

114   Environment, Science and Technology Commission (BEST) Permit with export under the

115   Bahamas Department of Agriculture permit numbers 39/2015, 28/2016, and 09/2017. Specimens

116   were collected from a variety of habitats over multiple years including from mangrove-adjacent

117   sediments from Wildcat Cove, FL in 2014, seagrass (*Halodule wrightii*, *Thalassia testudinum*,

118   and *Syringodium filiforme*) from Bokeelia, FL in 2014, algae and seagrass (*H. wrightii*, *T.*

119   *testudinum*, and *S. filiforme*) from Sugarloaf Key, FL in 2016, seagrass (*T. testudinum* and *S.*

120   *filiforme*) from Grahams Harbor, the Bahamas in 2016, mangrove-adjacent and seagrass (*H.*

121   *wrightii*, *T. testudinum*, and *S. filiforme*) from Pigeon Creek, the Bahamas in 2016 and 2017,

122   macroalgae and seagrass (*Ruppia maritima*) from Crescent Pond, the Bahamas in 2016 and 2017,

123   macroalgae from Moon Rock Pond, the Bahamas in 2016 and 2017, and no vegetative cover

124   from Pain Pond, the Bahamas in 2018. Sampling methods in Florida were described in Lim et al.

125   (2019, 2021). Sampling in the Bahamas was done using similar approaches, with the following

126   modifications: sediment was hand-dug and -sieved to 30–50 cm depth from within randomly

127   distributed quadrats measuring 0.5 m^2, rather than equally spaced quadrats oriented in transects

128   that were perpendicular to shore because sampling locations were not shoreline environments,

129   but instead a creek and inland lakes. Live-collected specimens were temporarily maintained in

130   Nasco Whirl-Pak bags with water from the habitat and maintained at ambient temperature before

131   dissection within six hours of collection. One gill and a portion of the foot tissue were separated

132   from the rest of the soft body parts and the shells. The gill and foot tissues were separately

133   placed in RNA*later* solution (rather than 100% molecular grade ethanol) and kept at 4 ºC for 24

134   hours before storage at -20 ºC for transport and until analysis at the University of Tennessee–

135   Knoxville. Dry shells and soft tissues stored in either ethanol or RNA*later* were catalogued at the

136   Museum of Geology, South Dakota School of Mines and Technology (SDSM).

137   All specimens were grouped by species assignment, and localities were pooled for

138   statistical analyses described in this work because of small and uneven sample sizes among

139   species. For example, some species had small sample sizes, such as *Anodontia alba* ($n = 6$),

140   *Lucina aurantia* ($n = 26$), and *Lucinisca nassula* ($n = 11$). While *Ctena orbiculata* was abundant

141   at one locality, it was represented by only one individual at two other localities. More common

142   taxa included *Codakia orbicularis*, *Ctena* sp., *Phacoides pectinatus*, and *Stewartia floridana*.

143 **Table 1:** List of specimens used in this study with associated locality, count (n), and South Dakota
144 School of Mines (SDSM) and Technology, Museum of Geology, accession numbers. All
145 specimens were used for geometric morphometric analysis unless otherwise noted. Specimens
146 used for phylogenetic data are also listed in Table 3.

Locality	n	SDSM Numbers
Anodontia alba		
Sugarloaf Key, Florida	6	134122*, 134126, 134127, 134129*, 134107, 134108
Codakia orbicularis		
Pigeon Creek, Bahamas	29	103116 – 103120, 115522, 115523, 115629, 115630, 115633 – 115635, 115639, 115644, 115648, 115655, 115656, 140433, 140448, 140449, 140818 – 140821, 140834, 140835, 140838, 140847, 140853
Sugarloaf Key, Florida	16	134069, 134078, 134079, 134081, 134082, 134083*, 134086, 134089, 134090, 134093, 134094, 134109, 134114 – 134116, 134138
Ctena orbiculata		
Bokeelia, Florida	1	111511
Pigeon Creek, Bahamas	1	140826
Sugarloaf Key, Florida	73	116881, 116883 – 116886, 116888 – 116890, 116892 – 116899, 116902 – 116905, 116907 – 116912, 116914 – 116916, 116920, 116921, 116923, 116924, 116927 – 116929, 116931 – 116937, 133849 – 133855, 133857, 133858, 134071 – 134075, 134091, 134092, 134099, 134100, 134110 – 134113, 134119, 134132 – 134136, 134139, 134140
Ctena sp.		
Crescent Pond, Bahamas	44	115660 – 115683, 140322 – 140339, 140350, 140351
Moon Rock Pond, Bahamas	86	115725 – 115744, 140359 – 140380, 140384 – 140389, 140391 – 140405, 140409 – 140430
Pain Pond, Bahamas	85	140455 – 140476, 140478 – 140499, 140501 – 140541
Pigeon Creek, Bahamas	10	115526, 115631*, 115632, 115647, 140432, 140434, 140442, 140810, 140846, 140852
Lucina aurantia		
Pigeon Creek, Bahamas	16	103122 – 103128, 115615, 115621, 115622, 115645, 140807 – 140809, 140827, 140829
Grahams Harbor, Bahamas	10	102773, 102774, 102782 – 102788, 115713
Lucinisca nassula		
Bokeelia, Florida	1	111515
Sugarloaf Key, Florida	10	134070, 134076, 134077, 134101, 134120, 134123 – 134125, 134130, 134131

147 *Shell broken, specimen not used in morphometric analysis
148
149
150

Table 1: (Continued)

Locality	n	SDSM Numbers
Phacoides pectinatus		
✳Wild Cat Cove, Florida	99	111051 – 111077, 111083 – 111098, 111100 – 111110, 111420 – 111458, 111459*, 111471, 111480, 111494, 111498, 111506
Stewartia floridana		
▽Bokeelia, Florida	140	110398 – 110415, 110417 – 110443, 110444*, 110445 – 110448, 110450 – 110477, 145704 – 145718, 145721 – 145768

*Shell broken, specimen not used in morphometric analysis
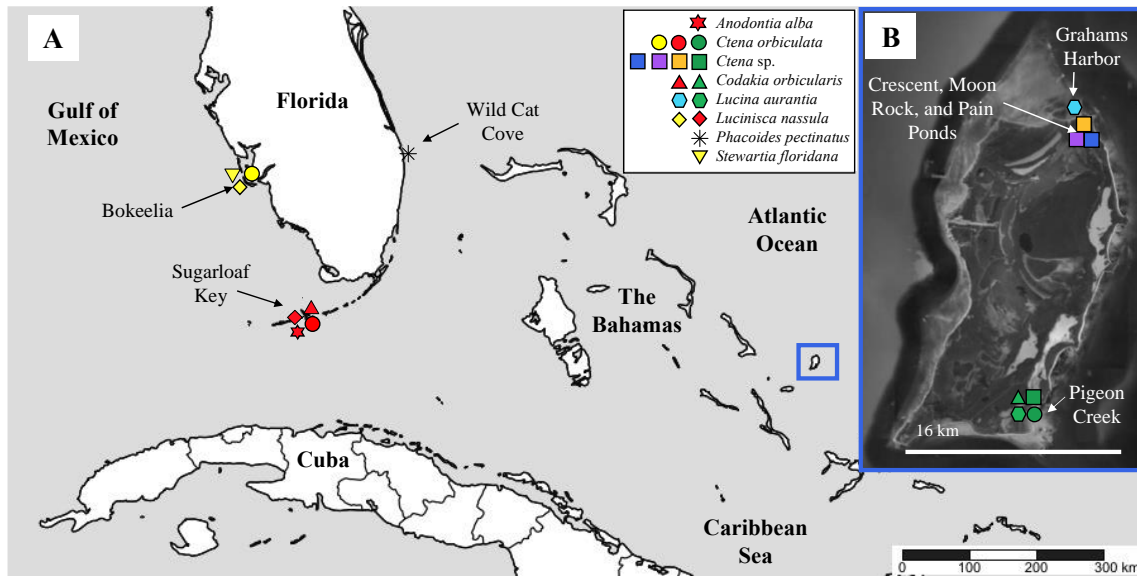
Figure 1: Map of the eight localities where the eight lucinid taxa were collected for this study. *Anodontia alba* (stars) were collected at Sugarloaf Key, Florida (Red), USA. Refer to Table 1 for the legend. Map A is from SimpleMappr (Shorthouse 2010) and map B is from Google Earth (2015).

162   DNA extraction, gene amplification, sequencing, and assembly

163   DNA was extracted at the University of Tennessee–Knoxville from approximately 25 mg

164   of gill and foot tissues, separately, from 62 specimens using the Qiagen DNeasy Blood & Tissue

165   Kits, following manufacturer instructions. DNA was diluted to 10–25 ng prior to PCR

166   amplification. Four genes were selected to be amplified and sequenced: the nuclear ribosomal

167   genes 18S rRNA and 28S rRNA, and the mitochondrial genes cytochrome b (cyt b) and

168   cytochrome oxidase I (COI). Previous lucinid molecular phylogenies indicated that 18S rRNA,

169   28S rRNA, and cyt b are phylogenetically informative genes (Williams et al. 2004; Taylor et al.

170   2011, 2013, 2014, 2016; Kuhara et al. 2014; Glover et al. 2016) so they are used here for

171   comparative purposes. While COI has not been used in lucinid phylogenies, it was selected for

172   this study due to its utility in population studies of other bivalves (Zanatta and Murphy 2008;

173   Tarnowska et al. 2010; Feng et al. 2011; Sanna et al. 2017). The 18S rRNA, 28S rRNA, cyt b,

174   and COI genes were amplified at Clemson University using specific primers for each gene

175   (Table 2). PCR was performed using similar conditions for all primers, except for $MgCl_2$

176   concentrations and primer annealing temperatures (see Table 2), in 20 µL volumes. Each

177   reaction mixture contained 10 µL of Bioline BIO-X-ACT™ Short Mix, 8.2 µL of H_2O (8.6 µL

178   of H_2O for 28S rRNA), 0.4 µL of 25 mM $MgCl_2$ (no additional $MgCl_2$ for 28S rRNA; see Table

179   2 for concentrations), 0.2 µL of 10 µM concentrations of forward and reverse primers, and 1 µL

180   of DNA. Thermal cycling was performed with an initial denaturation step for 2 minutes at 94 °C,

181   followed by 40 cycles of: 30 seconds at 94 °C, 30 seconds at the gene-specific annealing

182   temperature (Table 2), and 90 seconds at 72 °C; a final extension step was for 5 minutes at 72

183   °C. Gel electrophoresis was used to verify the PCR reactions, and successful PCR products were

184   purified using a QIAquick PCR Purification Kit (QIAGEN) to remove unwanted components.

185   Sanger Sequencing (Eton Biosciences, NC) was able to fully sequence the amplified products

186   with the two end primers.

187   Forward and reverse sequences were compared and overlapping sequences (to generate

188   contiguous sequences) were constructed in Sequencher 5.4.6 (Gene Codes Corporation, Ann

189   Arbor, MI, USA). Consensus sequence parameters were set to the following defaults: assembly

190   algorithm – dirty data, optimize gap replacement – use reAligner and prefer 3'gap placement,

191   minimum match percentage – 85, and minimum overlap – 20. Consensus sequences for the four

192   genes were deposited in GenBank (Benson et al. 2013; Sayers et al. 2020, 2021) and are listed in

193   Table 3. For Sanger sequencing of the 18S rRNA gene, only two of the four primers previously

194   used in studies (Taylor et al. 2011, 2016) were employed. As a result, the 18S rRNA genes did

195   not overlap and fragments with gaps were deposited. Similarly, amplification for some genes

196   was unsuccessful for some specimens (Table 3).

197   **Table 2:** PCR primers for the 18S rRNA, 28S rRNA, cyt *b*, and COI genes, with primer sequence,
198   annealing temperature, final magnesium chloride ($MgCl_2$) concentrations, and primer reference.

Gene/Primer	Sequence 5' → 3'	Annealing	[$MgCl_2$]	Reference
18S rRNA				
18S-5′ (Forward)	CTGGTTGATYCTGCC AGT	50 ℃	3.0 mM	Winnepenninckx et al. 1998
18S1100R (Reverse)	CTTCGAACCTCTGAC TTTCG	50 ℃	3.0 mM	Williams et al. 2003
28S rRNA				
LSU5 (Forward)	TAGGTCGACCCGCTG AAYTTAAGCA	55 ℃	2.0 mM	Littlewood et al. 2000
LSU1600R (Reverse)	AGCGCCATCCATTTT CAGG	55 ℃	2.0 mM	Williams et al. 2003
Cyt*b*				
cytB-F (Forward)	GRGGKGCTACKGTA ATTACTAA	50 ℃	3.0 mM	Taylor et al. 2008
cytB-R (Reverse)	AAATAYCAYTCNGG CTGRATATG	50 ℃	3.0 mM	Taylor et al. 2008
COI				

CO1490 (Forward)	GGTCAACAAATCATA AAGATATTGG	52 ℃	3.0 mM	Folmer et al. 1994
HC02198 (Reverse)	TAAACTTCAGGGTGA CCAAAAAATCA	52 ℃	3.0 mM	Folmer et al. 1994

199

Table 3: Taxa included in the analysis with associated localities, South Dakota School of Mines and Technology Museum of Geology (SDSM) catalog numbers, and GenBank accession numbers.

Taxa	Locality	SDSM	18S rRNA	28S rRNA	Cyt *b*	COI
Anodontia alba	Sugarloaf Key, Florida	134122	MK204749	MK190964	MK461261	—
	Sugarloaf Key, Florida	134126	MK204750	MK190965	MK461262	—
	Sugarloaf Key, Florida	134127	MK204751	MK190966	MK461263	—
	Sugarloaf Key, Florida	134129	MK204752	MK190967	MK461264	—
	Sugarloaf Key, Florida	134108	MK204753	MK190968	MK461265	—
Codakia orbicularis	Pigeon Creek Mouth, Bahamas	115522	MK204754	MK190969	MK461266	MK461210
	Pigeon Creek Mouth, Bahamas	115629	MK204755	MK190970	MK461267	MK461211
	Pigeon Creek Mouth, Bahamas	115630	MK204756	MK190971	MK461268	MK461212
	Pigeon Creek Mouth, Bahamas	115655	MK204757	MK190972	MK461269	MK461213
	Pigeon Creek Mouth, Bahamas	115656	MK204758	MK190973	MK461270	MK461214
	Sugarloaf Key, Florida	134069	MK204759	MK190974	MK461271	MK461215
	Sugarloaf Key, Florida	134083	MK204760	MK190975	—	—
	Sugarloaf Key, Florida	134093	MK204761	MK190976	MK461272	MK461216
	Sugarloaf Key, Florida	143800	MK204762	MK190977	MK461273	MK461217
	Sugarloaf Key, Florida	134114	MK204763	MK190978	MK461274	MK461218
Ctena orbiculata	Bokeelia, Florida	111511	MK204764	MK190979	MK461275	MK461219
	Pigeon Creek Mouth, Bahamas	140826	MK204784	MK190999	MK461295	—
	Sugarloaf Key, Florida	116885	MK204776	MK190991	MK461287	MK461231
	Sugarloaf Key, Florida	133857	MK204777	MK190992	MK461288	—
	Sugarloaf Key, Florida	133852	MK204778	MK190993	MK461289	MK461232
	Sugarloaf Key, Florida	116912	MK204779	MK190994	MK461290	MK461233
	Sugarloaf Key, Florida	116929	MK204780	MK190995	MK461291	—
Ctena sp.	Crescent Pond, Bahamas	115660	MK204766	MK190981	MK461277	MK461221
	Crescent Pond, Bahamas	115661	MK204767	MK190982	MK461278	MK461222
	Crescent Pond, Bahamas	115662	MK204768	MK190983	MK461279	MK461223
	Crescent Pond, Bahamas	115673	MK204769	MK190984	MK461280	MK461224
	Crescent Pond, Bahamas	115677	MK204770	MK190985	MK461281	MK461225

Table 3: (Continued)

Taxa	Locality	SDSM	18S rRNA	28S rRNA	cyt *b*	COI
Ctena sp.	Moon Rock Pond, Bahamas	115725	MK204771	MK190986	MK461282	MK461226
	Moon Rock Pond, Bahamas	115726	MK204772	MK190987	MK461283	MK461227
	Moon Rock Pond, Bahamas	115727	MK204773	MK190988	MK461284	MK461228
	Moon Rock Pond, Bahamas	115728	MK204774	MK190989	MK461285	MK461229
	Moon Rock Pond, Bahamas	115733	MK204775	MK190990	MK461286	MK461230
	Pain Pond, Bahamas	140460	MK204785	MK191000	MK461296	MK461237
	Pain Pond, Bahamas	140461	MK204786	MK191001	MK461297	MK461238
	Pain Pond, Bahamas	140462	MK204787	MK191002	MK461298	MK461239
	Pain Pond, Bahamas	140463	MK204788	MK191003	MK461299	MK461240
	Pain Pond, Bahamas	140464	MK204789	MK191004	MK461300	MK461241
	Pigeon Creek Mouth, Bahamas	115631	MK204765	MK190980	MK461276	MK461220
	Pigeon Creek Mouth, Bahamas	140434	MK204781	MK190996	MK461292	MK461234
	Pigeon Creek Mouth, Bahamas	140810	MK204782	MK190997	MK461293	MK461235
Lucina aurantia	Grahams Harbor, Bahamas	115713	MK204794	MK191009	MK461307	MK461248
	Pigeon Creek Mouth, Bahamas	115621	MK204790	MK191005	MK461303	MK461244
	Pigeon Creek Mouth, Bahamas	115622	MK204791	MK191006	MK461304	MK461245
	Pigeon Creek Mouth, Bahamas	115615	MK204792	MK191007	MK461305	MK461246
	Pigeon Creek Mouth, Bahamas	115645	MK204793	MK191008	MK461306	MK461247
	Pigeon Creek Mouth, Bahamas	140827	MK204795	—	MK461308	MK461249
Lucinisca nassula	Sugarloaf Key, Florida	134123	MK204796	MK191010	MK461301	MK461242
	Sugarloaf Key, Florida	134101	MK204797	MK191011	MK461302	MK461243
Phacoides pectinatus	Wildcat Cove, Florida	111076	MK204798	MK191012	MK461309	MK461250
	Wildcat Cove, Florida	111427	MK204799	MK191013	MK461310	MK461251
	Wildcat Cove, Florida	111420	MK204800	MK191014	MK461311	MK461252
	Wildcat Cove, Florida	111448	MK204801	MK191015	MK461312	MK461253
	Wildcat Cove, Florida	111457	MK204802	MK191016	MK461313	MK461254
Stewartia floridana	Bokeelia, Florida	110451	—	MK191017	—	—
	Bokeelia, Florida	110452	MK204803	—	MK461314	—
	Bokeelia, Florida	110453	MK204804	—	MK461315	—

Table 3: (Continued)

Taxa	Locality	SDSM	18S rRNA	28S rRNA	Cyt*b*	COI
Stewartia floridana	Bokeelia, Florida	110455	MK204805	MK191018	MK461316	MK461255
	Bokeelia, Florida	110432	MK204806	—	MK461317	MK461256
	Bokeelia, Florida	143801	MK204807	—	MK461318	MK461257
	Bokeelia, Florida	143803	MK204808	—	MK461319	MK461258
	Bokeelia, Florida	143808	MK204809	—	MK461320	MK461259
	Bokeelia, Florida	143805	MK204810	—	MK461321	MK461260
Parathyasira equalis		—	AM774482	AM779656	FR686685	AM706524

202

203   Molecular Phylogenetics

204   The ClustalW algorithm in MEGA7 (Kumar et al. 2016) was used to align sequences

205   with the following settings: gap opening penalty = 15, gap extension penalty = 7, and delay

206   divergent cutoff = 95%. Sequences were aligned to a reference sequence downloaded from

207   GenBank (AM774498 for *A. alba*, AM774500 for *C. orbicularis*, LT614692 for *C. orbiculata*

208   and *C. imbricatula*, FR686738 for *L. pensylvanica*, FR686736 for *L. nassula*, AM774503 for *P.*

209   *pectinatus*, and FR686749 for *S. floridana*). Gaps and poorly aligned regions were removed

210   using Gblocks server, version 0.91b (Castresana 2000; Talavera and Castresana 2007) with the

211   settings 'allow gaps within final blocks' and 'allow less strict flanking positions,' resulting in the

212   18S rRNA gene length being reduced from 2,351 bp to 929 base pairs (bp) (39% of the original

213   data), the 28S rRNA gene being reduced from 1,751 bp to 1,221 bp (69% of the original data),

214   the cyt *b* gene being reduced from 554 bp to 384 bp (69% of the original data), and the COI gene

215   being reduced from 827 bp to 669 bp (80% of the original data). Trimming significantly removed

216   gaps, particularly in the 18S rRNA sequences. *Parathyasira equalis* was selected as an outgroup

217   because all four genes had sequences available on GenBank and *P. equalis* belongs to

218   Thyasiridae, the closest sister family to Lucinidae.

219   Phylogenetic analyses were performed using Bayesian inference with MrBayes version

220   3.2.6 (Huelsenbeck and Ronquist 2001; Ronquist and Huelsenbeck 2003). Each gene was

221   analyzed individually, then all four genes were combined into a single dataset and analyzed.

222   Each dataset was run with using a Metropolis-coupled Markov chain Monte Carlo (MCMCMC)

223   with 4 chains (1 cold chain and 3 heated chains). The analyses were run for 10,000,000

224   generations, sampling at a frequency of 1,000 with the first 25% of trees discarded as burn-in.

225   Evolutionary models for each gene were selected using jModelTest (Guindon and Gascuel 2003;

226   Posada 2008; Darriba et al. 2012). The GTR + I + Γ substitution model (a General Time

227   Reversible substitution model with a proportion of invariable sites and a gamma shaped

228   distribution of rates across sites) was selected for all four genes. Consensus trees were produced

229   with associated branch lengths and posterior probabilities support values. Trees were visualized

230   and edited in FigTree v1.4.4 (Rambaut 2018).

231   <u>Geometric Morphometrics</u>

232   Two-dimensional geometric morphometrics (Bookstein 1992) were used to quantify the

233   shape of the anterior and posterior adductor muscle scars, inhalant channel, and valve outline.

234   The landmark configuration consisted of six Type 1 and 2 landmarks, as well as 52

235   semilandmarks (Figure 2). Type 1 landmarks represent specific local homologous features (e.g.,

236   the intersection of anterior muscle scar and pallial line) and Type 2 landmarks are local extremes

237   along curvatures (e.g., maximum curvature of dorsal margin of anterior adductor muscle scar). In

238   addition, semilandmarks were used to outline curves, which were resampled at equal distance.

239   Lucinid landmarks selected were as follows, clockwise from the beak (Figure 2): (1)

240   beak, (2) maximum curvature of dorsal margin of anterior adductor muscle scar, (3) intersection

241   of anterior muscle scar and pallial line, (4) maximum curvature of ventral margin of anterior

242   adductor muscle scar, (5) intersection of posterior adductor muscle scar and pallial line, and (6)

243   maximum curvature of dorsal margin of posterior adductor muscle scar. Semilandmarks include

244   twenty equidistance semilandmarks around the edge of the shell, two equidistance

245   semilandmarks between landmarks 2 and 3, five equidistance semilandmarks between landmarks

246   3 to 4, five equidistance semilandmarks between landmarks 2 and 4, ten equidistance

247   semilandmarks between landmarks 3 to 5, five equidistance semilandmarks between landmarks 5

248   and 6 along the exterior of the posterior adductor scar, and five equidistance semilandmarks

249   between landmarks 5 and 6 along the interior of the posterior adductor scar. Although hinge

250   features are often used for taxonomic identification, particularly at the genus level, the number

251   and orientation of interlocking cardinal and lateral teeth vary among taxa, preventing placement

252   of homologous landmarks across taxa.

253   Specimens were imaged at 600 or 1,200 dpi (for specimens smaller than 2 cm) using an

254   HP Scanjet 8300 laser scanner and digitized using tpsDig2 version 2.31 (Rohlf 2017). Cartesian

255   coordinates were superimposed using a Generalized Procrustes Analysis (GPA) in the gpagen

256   function of the 'geomorph' package (Adams and Otárola-Castillo 2013; Adams et al. 2021;

257   Baken et al. 2021) in R (R Core Team 2020). The GPA removes non-shape variation by

258   centering the landmark configurations to the origin of the reference configuration, scaling the

259   configurations to centroid size (CS), and rotating the configuration to a common reference form

260   (Gower 1975; Rohlf and Slice 1990; Zelditch et al. 2012). Semilandmarks were allowed to slide

261   along tangent planes between two adjacent landmarks to minimize Procrustes distances. The

262   resulting per-specimen landmark coordinates were used for subsequent morphometric analysis.

263   Ordination methods were used to visualize morphospace differences among species,

264   while also allowing any locality differences to be visualized using color-filled shapes. The

265   ordination methods include a Principal Components Analysis (PCA) using gm.prcomp in the

266   'geomorph' package and an Canonical Variates Analysis (CVA) using CVA in the 'Morpho'

267   package (Schlager 2017). Finally, to test for statistically significant differences in Procrustes

268   shape among species, a multivariate analysis of variance (MANOVA) using residual

269   randomization in permutation procedures (RRPP) (Collyer and Adams 2018, 2020) was

270   implemented using the procD.lm function in the 'geomorph' package. For any statistically

271   significant results, a post-hoc test was performed using the permudist function in the 'Morpho'

272   package.
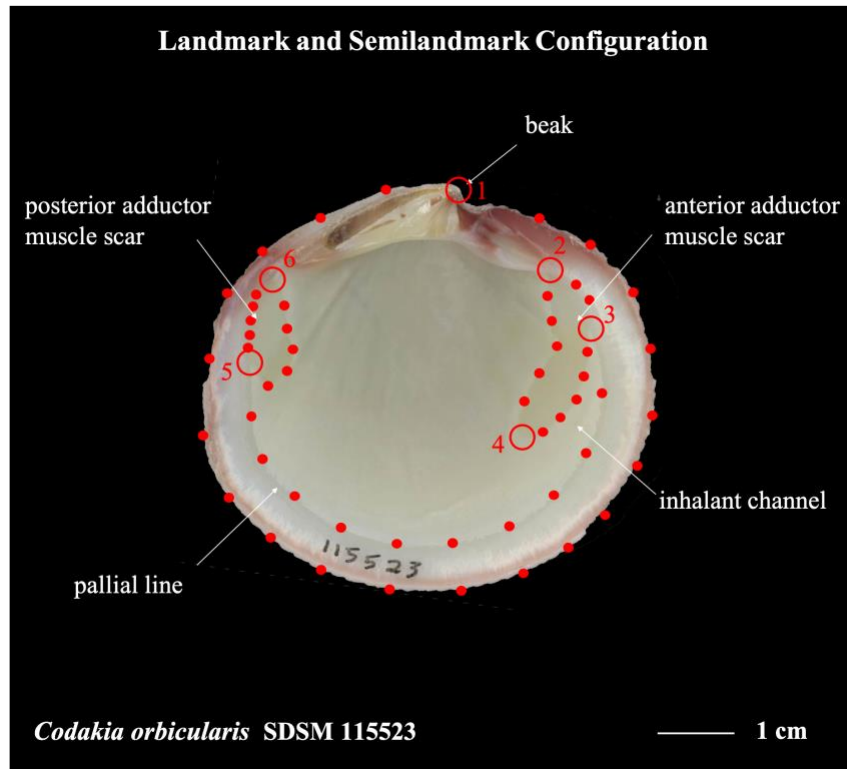
Figure 2: *Codakia orbicularis* specimen (SDSM 115523), with labelled landmarks (large open circles, numbered 1 through 6) and semilandmark curves (small filled circles) that were used in the analysis.

Phylogenetic Signal

279   For phylogenetic signal analyses, the phylogenetic and morphometric data were directly

280   combined after the following two steps: (1) the combined 18S rRNA, 28S rRNA, cyt *b*, and COI

281   gene phylogenetic tree was imported into R using the read.nexus function in the 'ape' package

282   (Paradis et al. 2004; Paradis and Schliep 2019) and branches were collapsed to show one

283   representative sequence from each species using the drop.tip function in the 'ape' package; (2)

284   the mean shell shape for each species was calculated from the geometric morphometric data

285   using the mshape function in the 'geomorph' package.

19

286   Phylogenetic signal of the shell shape and size were tested using K_{mult}, the multivariate

287   version of the K-statistic (Blomberg et al. 2003; Adams 2014). Tests for phylogenetic signal in

288   shell shape and size were performed using the physignal function in the 'geomorph' package.

289   The observed K value was compared to the null and assessed for significance, where K<1

290   indicates no phylogenetic signal, K=1 indicates a phylogenetic signal, and K>1 indicates a

291   phylogenetic signal greater than expected under Brownian motion (Blomberg et al. 2003; Adams

292   2014).

293   To visualize patterns of morphological variation in the shell shape data, three ordinations

294   were performed using variations of the gm.prcomp function in the 'geomorph' package. The first

295   ordination is a phylomorphospace analysis (PA), which is a standard PCA with the addition of

296   phylogenetic branches and estimated ancestral states projected into ordination space (Rohlf

297   2002; Sidlauskas 2008). If phylogenetic signal, as determined by K_{mult} is strong, then the first PC

298   axis of the PA should show the largest variation among the estimated ancestral trait values

299   (Collyer and Adams 2020). The second ordination method is a phylogenetic principal component

300   analysis (Phy-PCA), which produces a projection that is independent of phylogeny (Revell 2009;

301   Polly et al. 2013; Uyeda et al. 2015; Collyer and Adams 2020). The third ordination is a

302   phylogenetically aligned component analysis (PACA), which shows trends most associated with

303   phylogenetic signal (Collyer and Adams 2020). For PA, ordinary least squares (OLS) is used in a

304   standard principal components analysis (PCA), whereas for Phy-PCA, generalized least-squares

305   (GLS) is used to calculate a rates matrix and mean-centered residuals to account for phylogenetic

306   non-independence among taxa (Collyer and Adams 2020). PACA can use either OLS or GLS to

307   align residuals to the phylogenetic covariance matrix, here, GLS was used as it does not assume

308   phylogenetic independence (Collyer and Adams 2020; Collyer et al. 2021).

309   The first axis of all three ordination (PA, Phy-PCA, and PACA) were compared to one

310   another by calculating angles between the first components (Collyer and Adams 2018). To

311   determine if the first component of PA was a similar orientation to PACA, angles between

312   respective axes were calculated using the arccosine of vector cross-products using the

313   vec.cor.matrix function in the 'RRPP' package (Collyer and Adams 2018). The orientation of the

314   first axis of PA represents the axis with the greatest morphological variation, and if it is similar

315   to that of PACA, that would indicate that the axis of major morphologic variation is also the axis

316   with the strongest phylogenetic signal (Collyer and Adams 2020). For instances where

317   phylogenetic signal is not solely displayed in the axis of greatest morphological variation, or can

318   be attributed to multiple axes, shape interpretations need to encompass morphologic variation

319   across multiple axes. In this study, shape variation was examined using Thin-Plate Spline (TPS)

320   deformations of the mean shape of each species using the plotRefToTarget function in the

321   'geomorph' package.

322   **Results**

323   <u>Molecular Phylogenetics</u>

324   Single-gene phylogenetic trees inferred from 18SrRNA (Figure 3), 28S rRNA (Figure 4),

325   cyt *b* (Figure 5), and COI (Figure 6), along with the tree inferred with the combined datasets of

326   all four genes (18S rRNA, 28S rRNA, cyt *b*, and COI), resulted in congruent topologies (Figure

327   7) relative to previous work (Taylor et al. 2011, 2016). Overall, clade positions had strong

328   support (>98%) at the species-level for 28S rRNA (Figure 4), cyt *b* (Figure 5), COI (Figure 6),

329   and the combined gene tree (Figure 7).

330   As expected from the large gaps in 18S rRNA gene sequence data generated in this study,

331   as well as missing sequence data for some taxa, the resolution for some taxa was low and

332   exhibited numerous unresolved clades and polytomies, depending on the gene. Even with larger

333   datasets, taxonomic relationships among some subfamilies, like the Lucininae, are not well

334   resolved (Taylor et al. 2011; Taylor et al. 2016). From the gene trees, members of the Lucininae

335   were consistently placed within a single clade, but relationships among species varied,

336   particularly the placement of *S. floridana* and *P. pectinatus.* Moreover, the taxonomic positions

337   for *C. orbicularis*, *C. orbiculata* and *Ctena* sp. on the 18S rRNA gene tree were unresolved, as

338   were the *L. aurantia* and *L. nassula* clades. From the COI tree, other than the placement of *C.*

339   *orbicularis* as basal to both the Codakiinae and Lucininae subfamilies, all members of the

340   Codakiinae formed a clade that was fully resolved. The basal placement of *C. orbicularis* in the

341   COI tree may be an artifact because *A. alba* gene sequences were not successfully amplified

342   (Table 3).

343
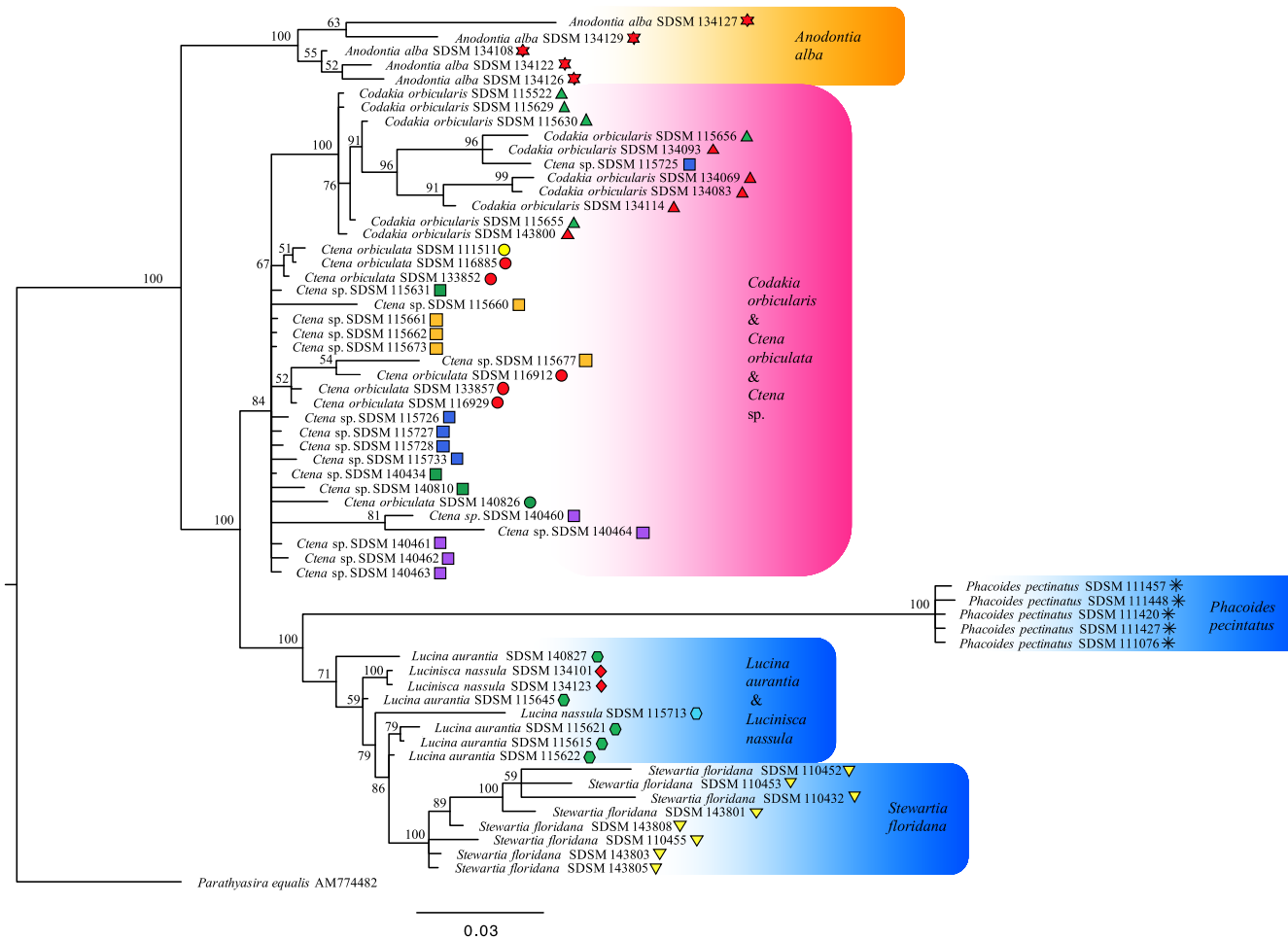
Figure 3: Bayesian inferred single gene tree for 18S rRNA sequences. Support values are posterior probabilities with branches less than 50% collapsed. Scale bar represents genetic distance for the number of substitutions per site. Symbols and colors next to taxa name explained in Figure 2.2. Colors indicate subfamilies designated in Taylor et al. (2011; 2016) as orange for Leucosphaerinae, pink for Codakiinae, and blue for Lucininae.

348
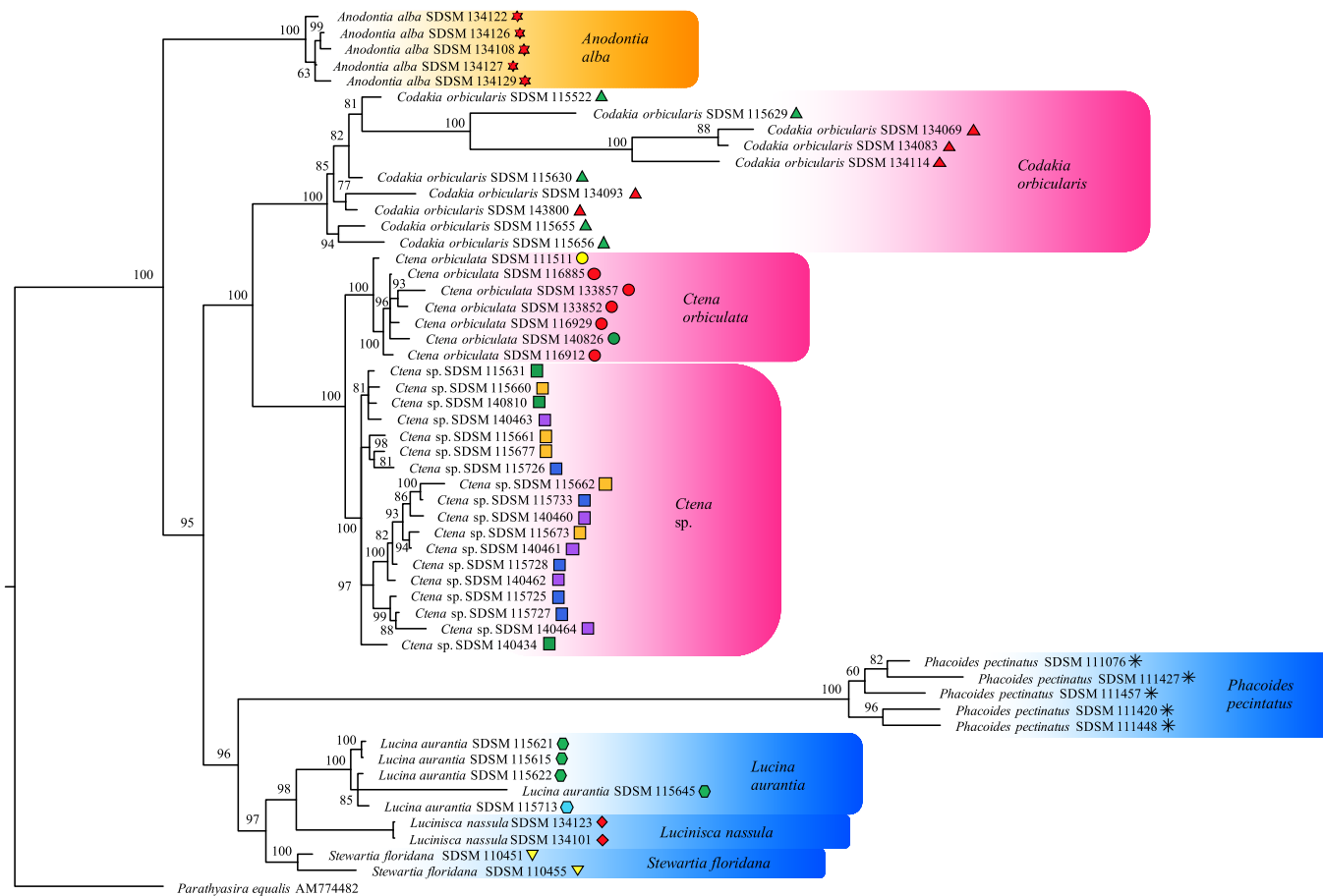
Figure 4: Bayesian inferred single gene tree for 28S rRNA sequences. Support values are posterior probabilities with branches less than 50% collapsed. Scale bar represents genetic distance for the number of substitutions per site. Symbols and colors next to taxa name explained in Figure 2.2. Colors indicate subfamilies designated in Taylor et al. (2011; 2016) as orange for Leucosphaerinae, pink for Codakiinae, and blue for Lucininae.

353
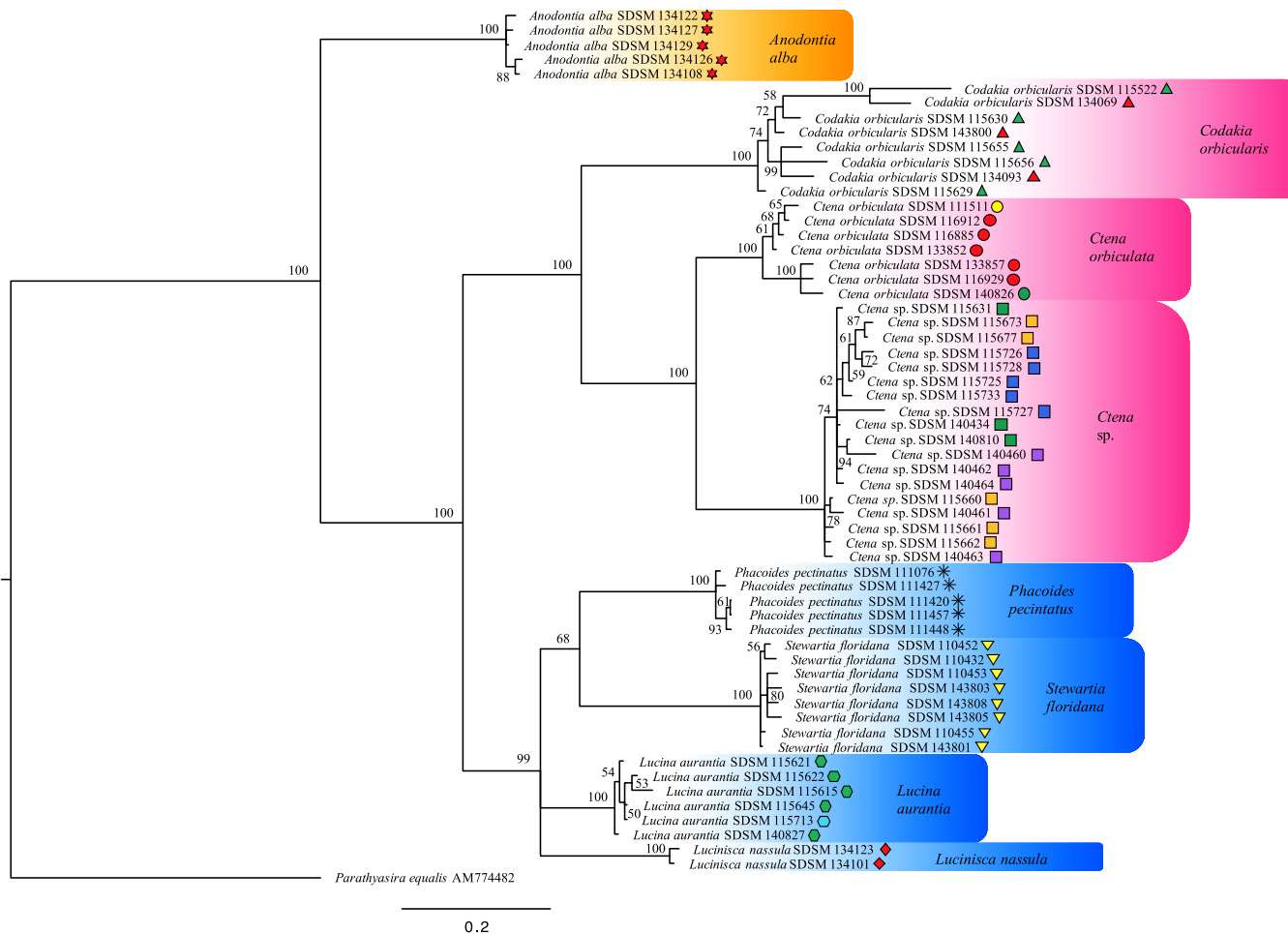
Figure 5: Bayesian inferred single gene tree for cyt *b* sequences. Support values are posterior probabilities with branches less than 50% collapsed. Scale bar represents genetic distance for the number of substitutions per site. Symbols and colors next to taxa name explained in Figure 2.2. Colors indicate subfamilies designated in Taylor et al. (2011; 2016) as orange for Leucosphaerinae, pink for Codakiinae, and blue for Lucininae.
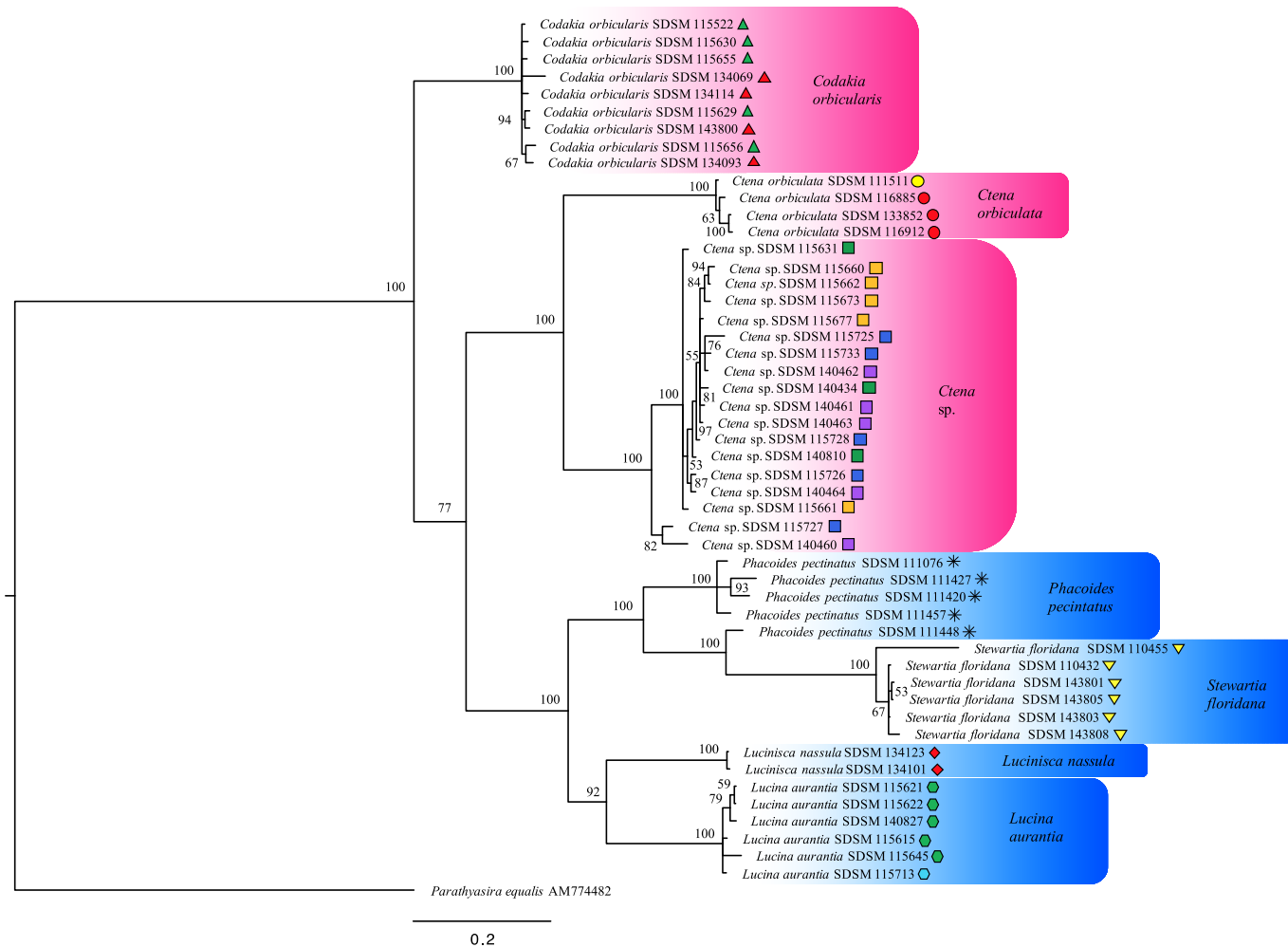
358
Figure 6: Bayesian inferred single gene tree for COI sequences. Support values are posterior probabilities with branches less than 50% collapsed. Scale bar represents genetic distance for the number of substitutions per site. Symbols and colors next to taxa name explained in Figure 2.2. Colors indicate subfamilies designated in Taylor et al. (2011; 2016) as pink for Codakiinae, and blue for Lucininae.
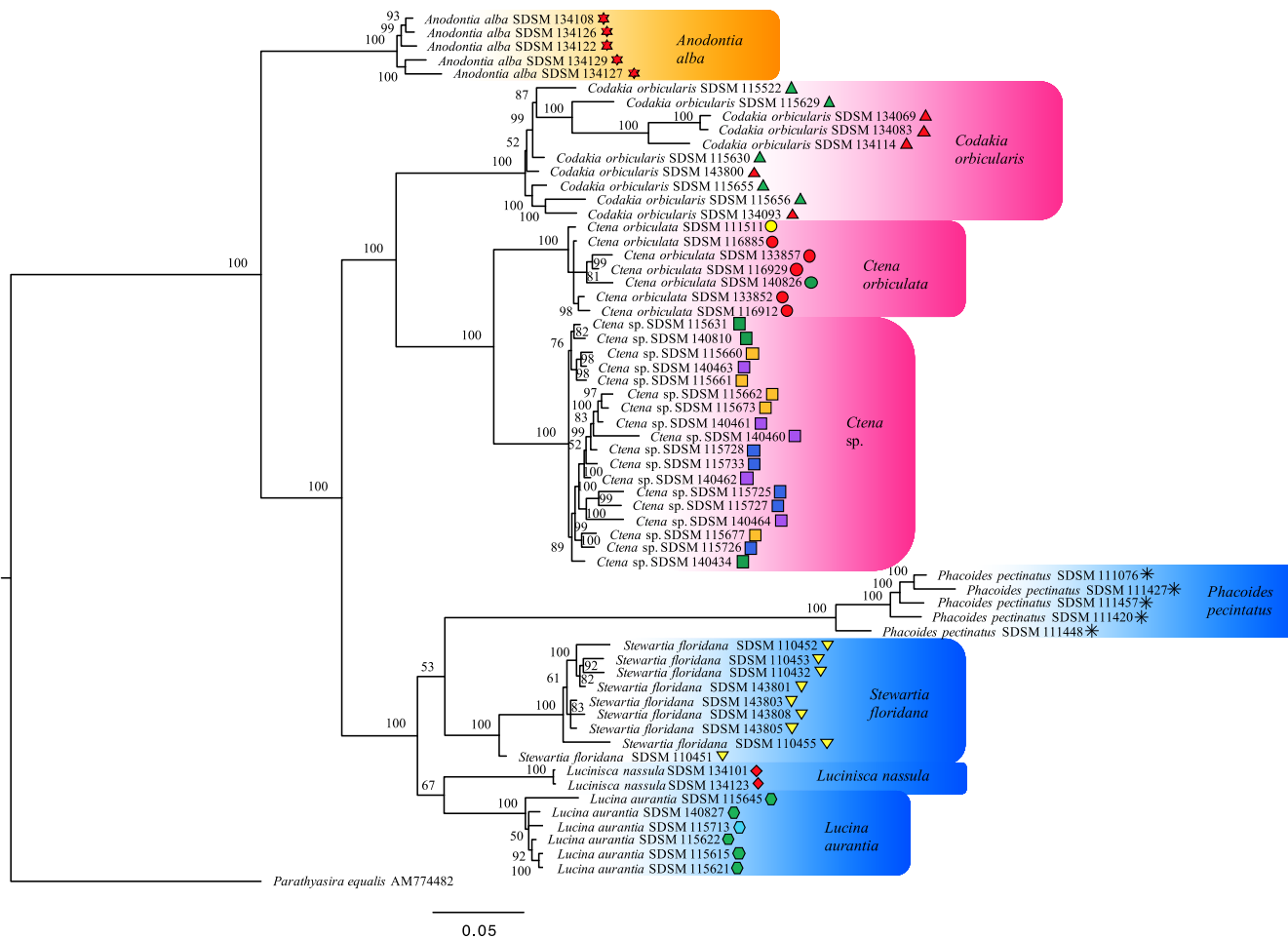
363
364
Figure 7: Combined gene tree produced by Bayesian analysis of concatenated 18S rRNA, 28S rRNA, cyt *b*, and COI sequences.
Support values are posterior probabilities with branches less than 50% collapsed. Scale bar represents genetic distance for the number
of substitutions per site. Symbols and colors next to taxa name explained in Figure 2.2. Colors indicate subfamilies designated in
Taylor et al. (2011; 2016) as orange for Leucosphaerinae, pink for Codakiinae, and blue for Lucininae.

Geometric Morphometrics

370   A PCA of the Procrustes shape coordinates resulted in the first two axes accounting for

371   over 78% of the variance (Figure 8). Though there was some scatter among the data, especially

372   for some individuals, PC1 vs. PC2 generally showed separation between species, but some

373   individuals of differing species overlapped each other. These patterns, including the distinct

374   scores of *P. pectinatus*, were similar to those of Anderson (2014) who used a simpler landmark

375   configuration (without semilandmarks).

376   The CVA (i.e., ordination with *a priori* species assignments) had more between-species

377   separation than the PCA for most taxa (Figure 9). CV1 and CV2 accounted for 74.15% of the

378   variation in the data. Classification accuracy based on *a priori* species assignment was overall

379   99% correct, with 621 out of 627 specimens being correctly assigned. The incorrectly assigned

380   specimens were three *Ctena* sp. assigned to *C. orbiculata* (1.34%) and three *C. orbiculata*

381   assigned to *Ctena* sp. ($n = 1$, 1.33%) and *C. orbicularis* ($n = 2$, 2.67%). There was overlap

382   among both morphologically similar taxa (e.g. *Ctena* sp. and *C. orbiculata*), and those that are

383   not morphologically similar (e.g. *A. alba* and *S. floridana*) (Figure 9). Note that there was some

384   misclassification ($n = 6$) for *Ctena* sp. and *C. orbiculata*, but not *A. alba* and *S. floridana*, as the

385   former pair of species are phylogenetically related, but the later pair are not.

386   MANOVA results indicated that there were significant differences in Procrustes shell

387   shape among species ($p = 0.001$), and post-hoc tests using a Holm (1979) adjusted p-value

388   indicated that all species were significantly different from one another in shape variation ($p =$

389   0.028), with the exception of *L. aurantia* and *L. nassula* (post-hoc $p = 0.124$), as well as *A. alba*

390   and *C. orbicularis* (post-hoc $p = 0.124$). The small sample size likely reduced the statistical

391   power of the post-hoc pairwise comparisons. Three of these taxa had small sample sizes (*A. alba*,

392   *n* = 4; *L. aurantia*, *n* = 26; *L. nassula,* *n* = 11) and shared similar shape spaces in both the PCA

393   (Figure 8) and CVA (Figure 9).

394   For *L. aurantia* and *L. nassula*, PCA and CVA results for the two taxa overlapped on

395   PC1 versus PC2 (explaining 78.07% of variance) and were adjacent to each other on CV1 versus

396   CV2 (explaining 74.15% of variance). This morphologic similarity likely reflects their relatively

397   close evolutionary relationship (Figure 7). In contrast, for *A. alba* versus *C. orbicularis*, *A. alba*

398   plotted between *C. orbicularis* and *S. floridana* on PC1 versus PC 2, whereas for CV1 vs. CV2,

399   *A. alba* specimens clustered within *S. floridana* on both axes and had comparable values with *C.*

400   *orbicularis* on CV2. In the Anderson (2014) study, *A. alba* plotted in a distinct space on CV1

401   versus CV2, adjacent to *C. orbicularis*, but that analysis did not include *S. floridana*.

402
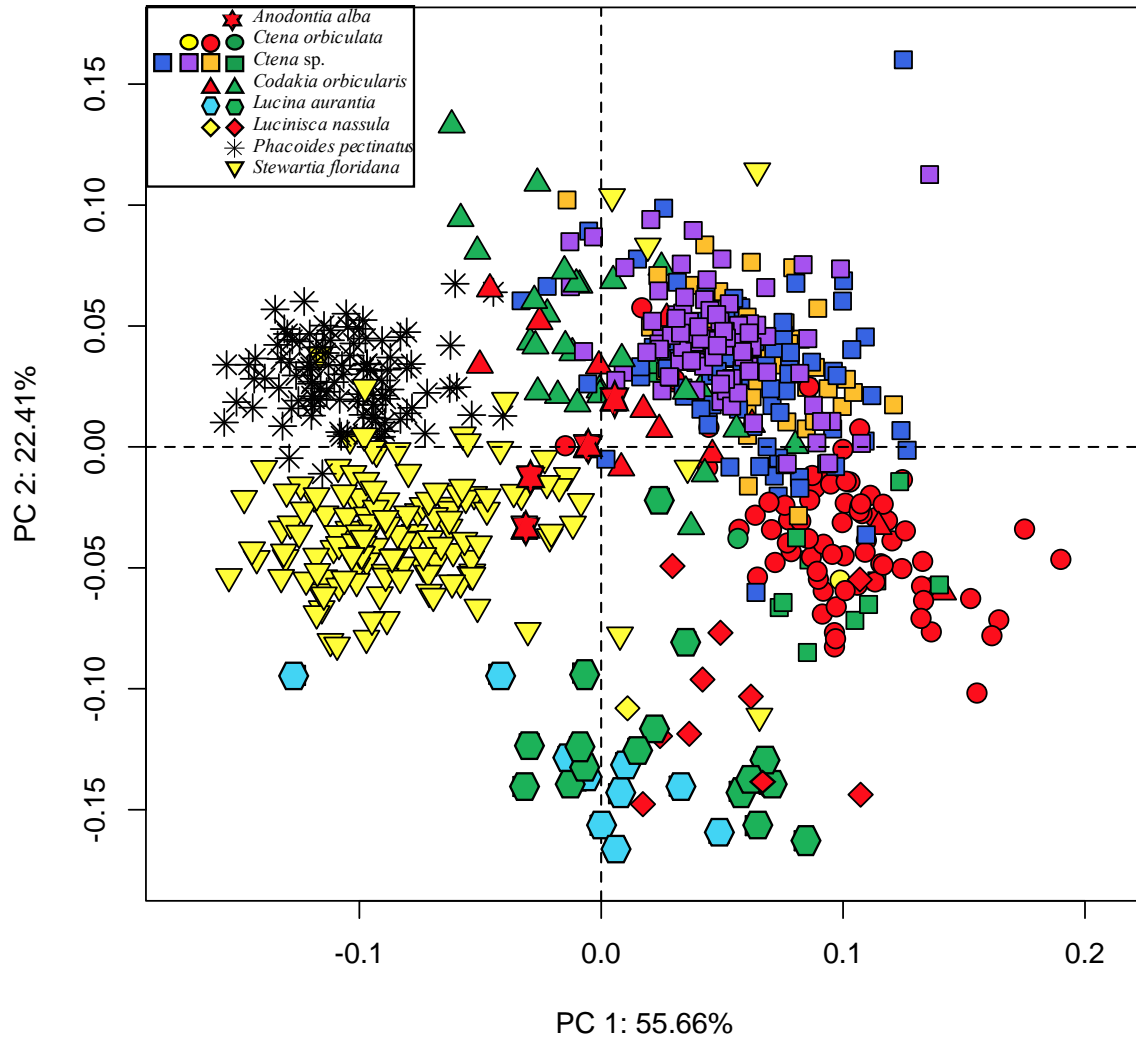
Figure 8: Principal Components Analysis (PCA) of shape variation for geometric morphometric data. Species are illustrated as symbols and localities are shown in the following colors: Bokeelia = yellow; Crescent Pond = orange; Grahams = light blue; Moon Rock Pond = blue; Pain Pond = purple; Pigeon Creek = green; Sugarloaf = red; Wild Cat Cove = black.

407

408
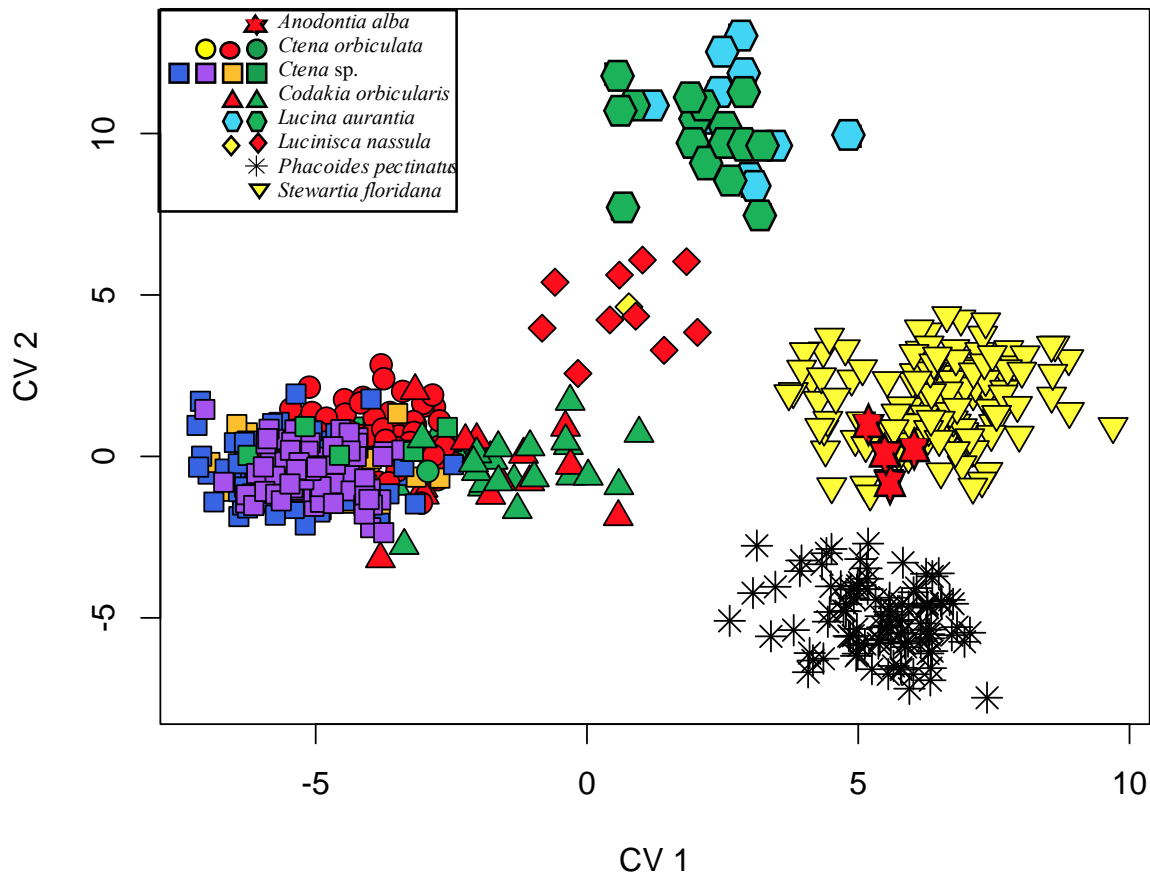
Figure 9: Canonical Variates Analysis (CVA) of shape variation for geometric morphometric data. Species are illustrated as symbols and localities are shown in the following colors: Bokeelia = yellow; Crescent Pond = orange; Grahams = light blue; Moon Rock Pond = blue; Pain Pond = purple; Pigeon Creek = green; Sugarloaf = red; Wild Cat Cove = black.

413

Phylogenetic Signal

415   Tests for phylogenetic signal indicated significance in shell shape (K_{mult} = 0.987, Z =

416   2.522, and p = 0.011) but not size (K_{mult} = 0.636, Z = -0.42, and p = 0.636). Phylogenetic signal

417   in shape was weaker than expected with a Brownian motion model of evolutionary divergence.

418   Morphospace ordination plots of the first two components of PA, Phy-PCA, and PACA (Figures

419   10, 11, and 12, respectively), in combination with the calculated arccosine of vector cross

420   products between axes, illustrated alignment with phylogenetic signal. There were no obvious

421   instances of morphologic convergence in the trees, as demonstrated by no overlapping branches

422   or nodes. The calculated angle between the first components of the PA and PACA was 55.839°,

423   indicating that the axis of PA with the most morphologic variation (PC1) did not align with the

424   axis aligned to the most phylogenetic signal (PAC1) (Figures 10 and 12).

425   Examination of univariate K_{mult} values for each component of PA, revealed that all eight

426   axes have univariate K_{mult} value near 1, indicating that each axis uniformly contributed to overall

427   phylogenetic signal. The calculated angle between the first components of the Phy-PCA and

428   PACA was 49.172°, meaning that the axis most independent of phylogenetic signal (Phy-PC1)

429   did not align with the axis aligned to the most phylogenetic signal (PAC1) (Figures 11 and 12).

430   PA and Phy-PCA were similarly oriented, with the calculated angle of 9.041° between the PC1

431   and Phy-PC1 (Figures 10 and 11). The axis with an orientation most aligned with phylogeny,

432   PAC1, compared to the axis with the next most phylogenetic signal, PAC2, illustrated how taxa

433   overlap in morphospace more on PAC1 than PAC2 (Figure 12). These results indicated that

434   PACA provided a more meaningful ordination compared to either PA or Phy-PCA due to the

435   distribution of phylogenetic signal across axes in the data being analyzed.

436   Comparison of PAC1 axis orientation with TPS representing mean shell shape explained

437   morphospace ordinations (Figure 13), and why shell shape differed significantly among taxa

438   (MANOVA, $p = 0.001$), with the exception of *L. aurantia* and *L. nassula* (post-hoc $p = 0.124$),

439   as well as *A. alba* and *C. orbicularis* (post-hoc $p = 0.124$). On PAC1, *A. alba* was the furthest on

440   that axis, and TPS revealed differences compared to the mean shell shape of other taxa, such as a

441   narrow, long inhalant channel, and a narrow shell margin indicative of shell inflation. On PAC1,

442   *C. orbicularis* and *P. pectinatus* shared similar morphospace; however, TPS indicated *S.*

443   *floridana* was more like *P. pectinatus* than *C. orbicularis* because of their overall outline shapes

444   and narrow, long inhalant channels. *S. floridana* exhibited slightly wider muscle scars. On PAC1,

445   *S. floridana*, *Ctena* sp., and *C. orbiculata* were close together in morphospace, although *C.*

446   *orbicularis* was more closely related to *Ctena sp.* and *C. orbiculata* compared to *S. floridana*.

447   TPS for *C. orbicularis, Ctena* sp., and *C. orbiculata* showed similar overall outline shapes, and a

448   very wide inhalant channel, although *Ctena* sp. and *C. orbiculata* had short inhalant channels

449   compared to *C. orbicularis* with a long inhalant channel. Lastly, *L. aurantia* and *L. nassula* had

450   similar TPS of overall outline shape and wide, short inhalant channels. Of note, the valves of

451   *Lucina* species in particular were more inflated that the other taxa used. As such, in the 2D

452   landmark configurations, there could have been some distortion when projecting size from 3D to

453   2D, and the calculated Procrustes variables could have skewed TPS reconstructions for these

454   species.

455
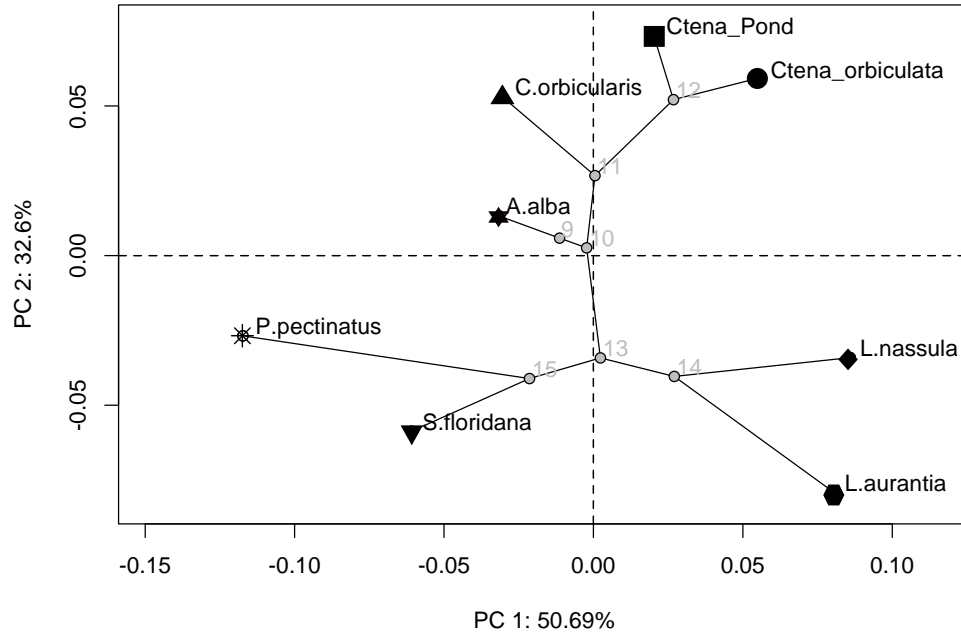
Figure 10: Phylomorphospace analysis (PA) illustrating the mean shell shape of species on components aligned to principal axes with ancestral states projected for phylogenetic nodes (Rohlf 2002; Sidlauskas 2008).

459

460
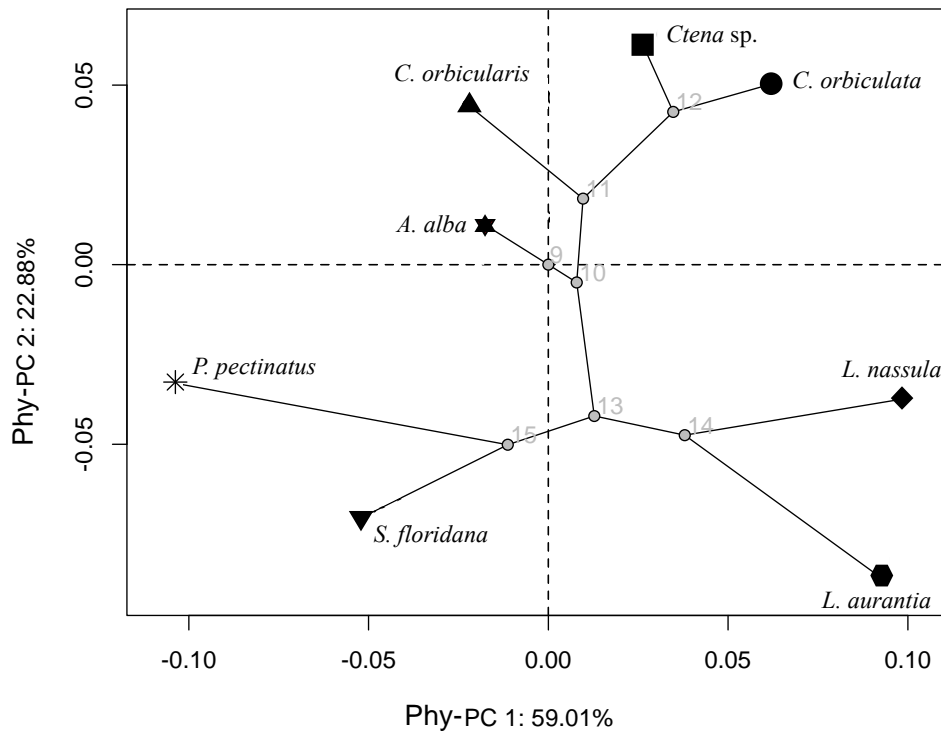
Figure 11: Phylogenetic principal component analysis (Phy-PCA) illustrating the mean shell shape of species on Phy-PC1, the first axis most independent of phylogeny, with ancestral states projected for phylogenetic nodes (Revell 2009).

34

464

465
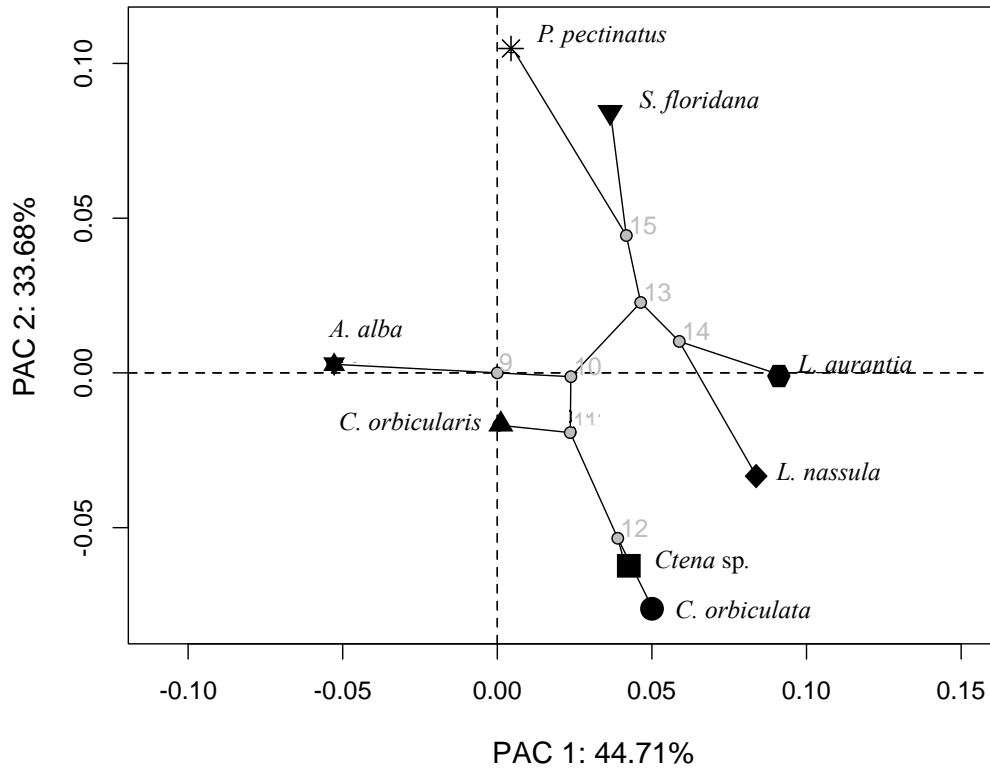
Figure 12: Phylogenetically aligned component analysis (PACA) illustrating the mean shell shape
of species on PAC1, the axis most aligned to phylogenetic signal, with ancestral states projected
for phylogenetic nodes (Collyer and Adams 2020).

469
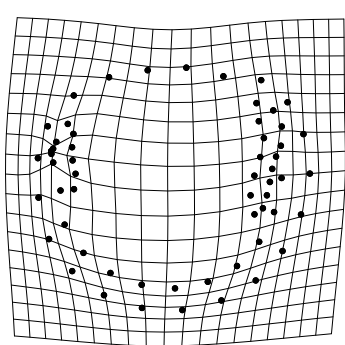
A. alba
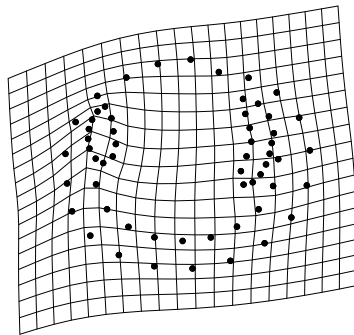
C. orbicularis
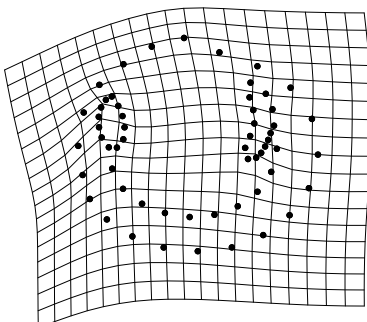
C. orbiculata
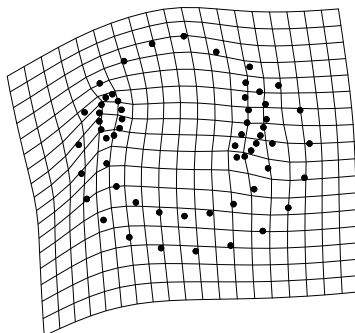
Ctena sp.
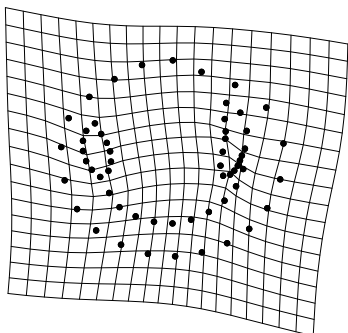
L. nassula
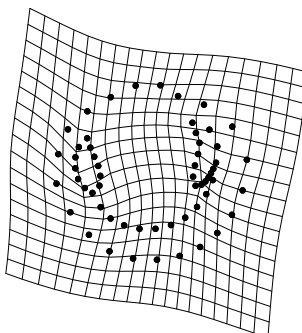
L. aurantia
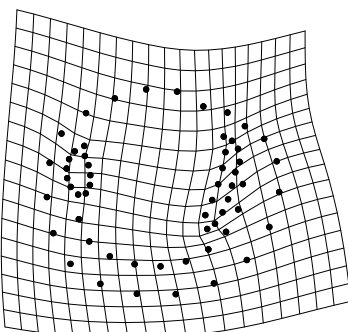
P. pectinatus

S. floridana

470
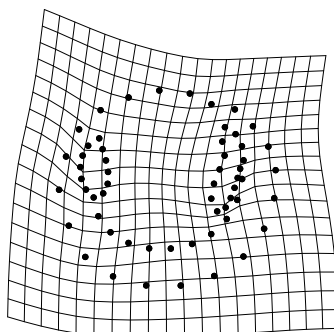
Figure 13: Thin-plate spline (TPS) analyses illustrate the deformation for the mean configuration of each species from the mean of the dataset.

471
472

Discussion

473

474   This study provides valuable insights into the ecological and evolutionary processes

475   influencing chemosymbiotic and infaunal bivalves. As the most species-rich family of

476   chemosymbiotic bivalves, Lucinidae have been extensively studied through molecular

477   approaches; however, their morphology has often been overlooked in recent phylogenetic

478   analyses (e.g., Williams et al. 2004; Taylor and Glover 2006; Taylor et al. 2011, 2016).

479   Morphology, however, remains a critical aspect of phylogenetics, as phenotypes are shaped by

480   both genotype and environmental interactions. The importance of this work lies in its

481   contribution to understanding the evolutionary relationships and morphological diversity within

482   Lucinidae, a family vital to nutrient cycling in coastal ecosystems.

483   Historically, morphological characters formed the foundation of most lucinid

484   phylogenetic studies (e.g., Bretsky, 1970, 1976; Chavan, 1969), despite the subjective nature of

485   such analyses. Recent studies have shifted toward molecular data, while largely ignoring

486   morphology (e.g. Williams et al. 2004; Taylor and Glover 2006; Taylor et al. 2011, 2016). This

487   work highlights the utility of geometric morphometrics, which considers shell shape as a whole

488   and enables statistical comparisons. Using a landmark-based approach, this study demonstrates

489   that shell morphology conveys significant phylogenetic signal within the Lucinidae. However,

490   the relationship between shape and phylogeny is complex, with no single feature definitively

491   characterizing specific clades.

492   <u>Phylogenetic Analysis and Molecular Congruence</u>

493   The phylogenetic trees generated in this study align closely with prior molecular analyses

494   (Taylor et al. 2016), confirming the robustness of the chosen genetic markers. However, some

495   incongruencies were noted within the subfamily Lucininae, notably involving *P. pectinatus* in

496 the 18S rRNA, 28S rRNA, and cyt *b* trees, *S. floridana* in the cyt *b* and combined tree, and *L.*

497 *nassula* in the cyt *b* tree. In molecular phylogenetic studies, *P. pectinatus* often exhibits a long

498 branch and unstable placement within the Lucininae (Taylor et al. 2011, 2013, 2016), a pattern

499 also reflected in this study. Similarly, the position of *Stewartia floridana* within the Lucininae

500 remains poorly resolved (Taylor et al. 2016), perhaps influenced by ecological or geographic

501 isolation.

502   In prior analyses that combined 18S rRNA, 28S rRNA and cyt *b* (Taylor et al. 2016), *P.*

503 *pectinatus* was placed more basally within the Lucininae. However, in this study, it appears as

504 the sister taxon to *S. floridana*. Additionally, *L. nassula* occupies a more basal position in the cyt

505 *b* tree of Taylor et al. (2016), which contrasts with its more derived placement alongside *Lucina*

506 *aurantia* in other analyses by Taylor et al (2016), and in the trees reconstructed in this study.

507 While combining multiple markers generally enhances resolution, discrepancies between

508 individual and combined trees suggest that other genetic markers or genome-wide approaches

509 may provide greater clarity. Moreover, environmental and morphological factors could play a

510 role; for example, *P. pectinatus* is often associated with specific sedimentary habitats that may

511 exert selective pressures influencing its molecular signals. These findings highlight the need for

512 integrative approaches combining genomic, ecological, and morphological data to refine the

513 phylogenetic placement of these taxa. Future studies might also explore the role of functional

514 traits in shaping the evolutionary history of Lucinidae, contributing to a broader understanding of

515 diversification in chemosymbiotic bivalves.

516 Detection of Phylogenetic Signal

517   This study identifies significant phylogenetic signal in shell shape (Kmult = 0.987),

518 demonstrating that morphology is phylogenetically informative. However, the signal is

519   distributed across the entire landmark configuration rather than attributable to a single feature, as

520   evidenced by thin-plate spline analyses.

521   The application of three ordination analyses (PA, Phy-PCA, and PACA) reveal that

522   different subfamilies of Lucinidae occupy distinct regions in shape space, reinforcing the notion

523   that shell morphology can effectively differentiate between higher taxonomic levels within this

524   group. For instance, TPS analysis indicated that species within the Codakiimae (*C. orbicularis*,

525   *C. orbiculata*, and *Ctena* sp.) share a similar overall outline shape and feature the widest inhalant

526   channel of the taxa analyzed here, suggesting a conserved morphotype that may be linked to

527   ecological factors such as feeding or habitat preferences.. Similarly, within the Lucininae,

528   species pairs such as *L. aurantia* and *L. nassula,* and to a lesser extent, *S. floridana* and *P.*

529   *pectinatus*, are similar in shell outline and inhalant channel shape. These findings emphasize that

530   both external shell outline and internal morphological structures, such as the inhalant channel,

531   contribute to the phylogenetic signal.

532   <u>Insights into Morphological Evolution</u>

533   This study documents significant phylogenetic signal in lucinid shell shape based on a

534   landmark configuration that emphasizes muscle scars, the inhalant channel, and valve outline.

535   Notably, univariate K values near 1 for each PA component indicate that each axis uniformly

536   contributes to overall phylogenetic signal. However, the axis with the most morphologic

537   variation (PC1) does not align with the axis aligned to the most phylogenetic signal (PAC1) ,

538   underscoring the complexity of shape evolution in lucinids. Furthermore, the absence of

539   overlapping branches or nodes in the resulting morphospace analyses suggest there are no

540   obvious instances of morphologic convergence in the taxa studied. These findings highlight that

541   phylogenetic signal arises from the entire landmark configuration rather than being confined to a

542   single morphological feature. For instance, in other taxa such as amphibians (Adams, 2014) and

543   fishes (Friedman et al., 2021), landmark-based studies have demonstrated that phylogenetic

544   signal is often a product of multiple integrated traits rather than isolated features. This integrative

545   perspective supports the notion that evolutionary pressures act on organisms as functional and

546   developmental units, where traits evolve together as part of a coordinated response to selection

547   pressures (Klingenberg, 2010). In lucinids, the lack of a single dominant feature driving

548   phylogenetic signal further underscores the importance of studying morphology at the whole-

549   organism level. Features such as shell outline, muscle scars, and the inhalant channel likely

550   represent a mosaic of traits shaped by a combination of lineage history and ecological

551   adaptations. This comprehensive approach is essential for resolving complex evolutionary

552   relationships in morphologically diverse taxa like the Lucinidae.

553   Comparisons with other taxa provide a broader context for interpreting the evolutionary

554   drivers of lucinid morphology. For example, the calculated angle between the first PA and

555   PACA axes ranged from ~4.5° for salamanders (Baken and Adams 2019), 19.4° for marine

556   fishes (Friedman et al. 2021), ~34.5° for surgeonfish (Friedman et al. 2016), and 58.7°

557   freshwater fishes (Friedman et al. 2021). These angles reflect the alignment between

558   morphological diversification and phylogenetic signal. A lower angle, as seen in marine fishes,

559   suggests that shape diversification proceeded along a trajectory aligned with phylogenetic signal

560   (Friedman et al. 2021). Conversely, a higher angle, such as in freshwater fishes, was interpreted

561   to mean that ecological signal was a strong driver of diversification, particularly because

562   freshwater lineages occupied a densely pack morphospace (Friedman et al. 2021).

563   In lucinids, the relatively high angle observed in this study, coupled with the lack of

564   densely packed morphospace clustering, suggests that both ecology and phylogenetic factors

565   play significant roles in shaping the morphology of these taxa. The distribution of phylogenetic

566   signal across the landmark configuration indicates that evolutionary lineage constraints

567   contribute broadly to the overall shape, while ecological factors likely drive the finer-scale

568   variation observed among taxa. This is consistent with patterns seen in other morphologically

569   and ecologically diverse clades, where both phylogenetic heritage and ecological niche

570   specialization shape morphological traits (Friedman et al., 2021; Klingenberg, 2010; Adams,

571   2014).

572   For lucinids, ecological factors such as sediment grain size, burrowing depth, and the

573   nature of symbiotic relationships with sulfur-oxidizing bacteria may exert strong selective

574   pressures on valve morphology, particularly features like shell outline and the inhalant channel.

575   Adaptations to specific sediment types or oxygen levels, for instance, might influence shell

576   thickness and shape (Seilacher, 1985; Stanley and Trueman, 1988; Oschmann, 1993;

577   Tomašových, 2018), while symbiotic interactions could drive internal morphological changes to

578   optimize nutrient exchange. These ecological pressures work with with phylogenetic constraints,

579   resulting in a morphospace that reflects a balance between lineage-specific traits and adaptive

580   responses to environmental challenges. By emphasizing the interplay of phylogeny and ecology,

581   this study highlights the importance of integrating these perspectives to fully understand the

582   morphological evolution of chemosymbiotic bivalves. Such integrative approaches not only

583   provide insights into the evolutionary history of lucinids but also inform broader questions about

584   how environmental and genetic factors interact to shape biodiversity in marine ecosystems.

585   This study bridges molecular and morphological perspectives, demonstrating that lucinid

586   shell shape captures phylogenetic signal despite complex ecological and evolutionary influences.

587   The integration of quantitative morphological methods with molecular phylogenetics paves the

588   way for more comprehensive studies of other chemosymbiotic or infaunal bivalves. This

589   approach provides valuable insights into the broader ecological and evolutionary processes that

590   could apply to other chemosymbiotic or infaunal bivalve systems.

591   **Data Availability**

592   All the original data and scripts necessary to reproduce the analyses reported in this study

593   can be accessed through Dryad Digital Repository: http://dx.doi.org/10.5061/dryad.70rxwdc7t

594   and Zenodo: https://doi.org/10.5281/zenodo.14649182. Sequence data are available from

595   GenBank under accession numbers found in Table 3.

596   **Acknowledgements**

611

612   **References**

613   Adams, D. C. 2014. A generalized K statistic for estimating phylogenetic signal from shape and

614   other high dimensional multivariate data. Systematic Biology 63:685–697.

615   https://doi.org/10.1093/sysbio/syu030

616   Adams, D. C. and E. Otárola-Castillo. 2013. geomorph: an R package for the collection and

617   analysis of geometric morphometric shape data. Methods in Ecology and Evolution 4:393-

618   399. https://doi.org/10.1111/2041-210X.12035

619   Adams, D. C., M. L. Collyer, A. Kaliontzopoulou, and E. K. Baken. 2021. Geomorph: Software

620   for geometric morphometric analyses. R package version 4.0. https://cran.r-

621   project.org/package=geomorph

622   Allen, J. A. 1958. On the basic form and adaptations to habitat in the Lucinacea

623   (Eulamellibranchia). Philosophical Transactions of the Royal Society B 684:421–484.

624   https://doi.org/10.1098/rstb.1958.0010

625   Anderson, L. C. 2014. Relationships of internal shell features to chemosymbiosis, life position,

626   and geometric constraints within the Lucinidae (Bivalvia), *in* D. I. Hembree, B. F. Platt, and J.

627   J. Smith, eds., Experimental Approaches to Understanding Fossil Organisms. Springer, p. 49-

628   72.

629   Baken, E. K., and D. C. Adams. 2019. Macroevolution of arboreality in salamanders. Ecology

630   and Evolution 9(12): 7005-7016. https://doi.org/10.1002/ece3.5267

631   Baken, E. K., M. Collyer, A. Kaliontzopoulou, and D. C. Adams. 2021. geomorph v4.0 and

632   gmShiny: enhanced analytics and a new graphical interface for a comprehensive

633   morphometric experience.

634   Benson, D. A., M. Cavanaugh, K. Clark, I. Karsch-Mizrachi, D. J. Lipman, J. Ostell, and E. W.

635   Sayers. 2013. GenBank. Nucleic Acids Research 41: D36-42.

636   https://doi.org/10.1093/nar/gks1195

637   Blomberg, S. P., T. Garland Jr, and A. R. Ives. 2003. Testing for phylogenetic signal in

638   comparative data: behavioral traits are more labile. Evolution 57:717–745.

639   https://doi.org/10.1111/j.0014-3820.2003.tb00285.x

640   Bookstein, F. L. 1992. Morphometric tools for landmark data. Geometry and Biology.

641   Cambridge University Press, New York.

642   Bretsky, S. S. 1970. Phenetic and phylogenetic classifications of the Lucinidae (Mollusca,

643   Bivalvia). Bulletin of the Geological Institution of the University of Upsala 2:5-23.

644   Bretsky, S. S. 1976. Evolution and classification of the Lucinidae (Mollusca; Bivalvia).

645   Palaeontographica Americana 8:219-337.

646   Castresana, J. 2000. Selection of conserved blocks from multiple alignments for their use in

647   phylogenetic analysis. Molecular Biology and Evolution 17:540-552.

648   https://doi.org/10.1093/oxfordjournals.molbev.a026334

649   Chavan, A. 1969. Superfamily Lucinacea Fleming, 1828. In Moore RC (ed) Treatise on

650   Invertebrate Paleontology, Part N, Mollusca 6, Bivalvia, Vol 2. Boulder, Colorado:

651   Geological Society of America and University of Kansas, N491-N518.

652   Christie, M., C. R. Congreve, and M. E. Patzkowsky. 2016. Phylogenetic diversity of the

653   Lucinidae in the Western Atlantic using fossils and molecules. Geological Society of America

654   Abstracts with Programs 48:7. https://doi.org/10.1130/abs/2016AM-286423

655   Christie, M. 2017. Biogeographic, Functional, and Phylogenetic Consequences of Climate

656   Change for Pliocene to Modern Marine Mollusks in the Western Atlantic. The Pennsylvania

657   State University. ProQuest Dissertations Publishing. Pp. 224.

658   https://www.proquest.com/dissertations-theses/biogeographic-functional-

659   phylogenetic/docview/2448407787/se-2?accountid=10003

660   Collyer, M. L. and D. C. Adams 2018. RRPP: An R package for fitting linear models to high-

661   dimensional data using residual randomization. Methods in Ecology and Evolution 9(7):1772-

662   1779. https://doi.org/10.1111/2041-210X.13029

663   Collyer, M. L. and D. C. Adams. 2020. Phylogenetically aligned component analysis. Methods

664   in Ecology and Evolution 12(2):359-372. https://doi.org/10.1111/2041-210X.13515

665   Collyer, M. L., E. K. Baken, and D. C. Adams. 2021. A standardized effect size for evaluating

666   and comparing the strength of phylogenetic signal. Methods in Ecology and Evolution 00:1-

667   16. https://doi.org/10.1111/2041-210X.13749

668   Darriba, D., G. L. Taboada, R. Doallo, and D. Posada. 2012. jModelTest 2: more models, new

669   heuristics and parallel computing. Nature Methods 9:772. https://doi.org/10.1038/nmeth.2109

670   Dando, P. R., S. A. Ridgway, and B. Spiro. 1994. Sulphide 'mining' by lucinid bivalve molluscs:

671   demonstrated by stable sulphur isotope measurements and experimental models. Marine

672   Ecology Progress Series 107:169-175. https://www.jstor.org/stable/24844788

673   Distel, D. L., and H. Felbeck. 1988. Pathways of inorganic carbon fixation in the endosymbiont-

674   bearing lucinid clam *Lucinoma aequizonata*. Part 2. Analysis of the individual contributions

675   of host and symbiont cells to inorganic carbon assimilation. Journal of Experimental Zoology

676   vol 247 issue 1 pp 11-22. https://doi.org/10.1002/jez.1402470102

677   Feng, Y., Q. Li, L. Kong, and X. Zheng. 2011. DNA barcoding and phylogenetic analysis of

678   Pectinidae (Mollusca: Bivalvia) based on mitochondrial COI and 16S rRNA genes. Molecular

679   Biology Reports 38:291–299. https://doi.org/10.1007/s11033-010-0107-1

680   Fiala-Médioni and Felbeck, H. 1990. Autotrophic processes in invertebrate nutrition: bacterial

681   symbiosis in bivalve molluscs, *in* R. K. H. Kinne, E. Kinne-Saffran, K. W. Beyenbach, eds.,

682   Comparative Physiology, Vol. 5, KargerBerlin, p. 49–69.

683   Folmer, O., M. Black, W. Hoeh, R. Lutz, and R. Vrijenhoek. 1994. DNA primers for

684   amplification of mitochondrial cytochrome c oxidase subunit I from diverse metazoan

685   invertebrates. Molecular Marine Biology and Biotechnology 3:294-299.

686   Friedman, S. T., S. A. Price, A. S. Hoey, and P. C. Wainwright. 2016. Ecomorphological

687   convergence in planktivorous surgeonfishes. Journal of Evolutionary Biology 29(5):965-978.

688   https://doi.org/10.1111/jeb.12837

689   Friedman, S. T., M. L. Collyer, S. A. Price, and P. C. Wainwright. 2021. Divergent processes

690   drive parallel evolution in marine and freshwater fishes. Systematic Biology syab080.

691   https://doi.org/10.1093/sysbio/syab080

692   Gaillard, C., M. Rios, Y. Rolin, and M. Roux. 1992. Fossil chemosynthetic communities related

693   to vents and seeps in sedimentary basins: The pseudobioherms of southeastern France

694   compared to other world examples. PALAIOS 7:451–465. https://doi.org/10.2307/3514829

695   Glover, E. A., and J. D. Taylor. 2007. Diversity of chemosymbiotic bivalves on coral reefs:

696   Lucinidae of New Caledonia and Lifou (Mollusca, Bivalvia). Zoosystema 29:109-181.

697   Glover, E. A., S. T. Williams, and J. D. Taylor. 2016. Lucinid bivalves of Singapore and their

698   relationships (Bivalvia: Lucinidae). Raffles Bulletin of Zoology Supplement 34:165-191.

699   Google Earth. 2015. 24°01'58"N, 74°29'08"W. Elevation 0ft. Imagery date: 12/13/2015.

700   Gower, J. C. 1975. Generalized Procrustes analysis. Psychometrika 40:33-51.

701   https://doi.org/10.1007/BF02291478

702   Guindon, S., and O. Gascuel. 2003. A simple, fast and accurate method to estimate large

703   phylogenies by maximum-likelihood. Systematic Biology 52:696-704.

704   https://doi.org/10.1080/10635150390235520

705   Holm, S. 1979. A simple sequentially rejective multiple test procedure. Scandinavian Journal of

706   Statistics 6:65–70.

707   Hopkins, M. J. 2016. Magnitude versus direction of change and the contribution of

708   macroevolutionary trends to morphological disparity. Biological Journal of the Linnean

709   Society 118:116-130. https://doi.org/10.1111/bij.12759

710   Huelsenbeck, J. P. and F. Ronquist. 2001. MRBAYES: Bayesian inference of phylogeny.

711   Bioinformatics 17:754-755. https://doi.org/10.1093/bioinformatics/17.8.754

712   Kiel S., K. A. Campbell, and C. Gaillard. 2010. New and little known mollusks from ancient

713   chemosynthetic environments. Zootaxa 2390:26–48. https://doi.org/10.11646/zootaxa.2390.1.2

714   Klingenberg, C. P. 2010. Evolution and development of shape: Integrating quantitative

715   approaches. Nature Reviews Genetics 11:623-635. https://doi.org/10.1038/nrg2829

716   Kuhara, T., Y. Kano, K. Yoshikoshi, and J. Hashimoto. 2014. Shell morphology, anatomy and

717   gill histology of the deep-sea bivalve *Elliptiolucina ingens* and molecular phylogenetic

718   reconstruction of the chemosynthetic family Lucinidae. Venus 72:13-27.

719   Kumar, S., G. Stecher, and K. Tamura. 2016. MEGA7: Molecular evolutionary genetics analysis

720   version 7.0 for bigger datasets. Molecular Biology and Evolution 33:1870-1874.

721   https://doi.org/10.1093/molbev/msw054

722   Liljedahl, L. 1992. The Silurian *Ilionia prisca*, oldest known deep-burrowing suspension-feeding

723   bivalve. Journal of Paleontology 66(2): 206–210. https://doi.org/10.1017/S0022336000033722

724   Lim, S. J., B. G. Davis, D. E. Gill, J. Walton, E. Nachman, A. S. Engel, L. C. Anderson, and B.

725   J. Campbell. 2019a. Taxonomic and functional heterogeneity of the gill microbiome in a

726   symbiotic coastal mangrove lucinid species. ISME 13:902-920.

727   https://doi.org/10.1038/s41396-018-0318-3

728   Lim, S. J., B. G. Davis, D. E. Gill, J. Swetenburg, L. C. Anderson, A. S. Engel, and B. J.

729   Campbell. 2021. Gill microbiome structure and function in the chemosymbiotic coastal

730   lucinid *Stewartia floridana*. FEMS Microbiology Ecology 97(4):fiab042.

731   https://doi.org/10.1093/femsec/fiab042

732   Littlewood, D. T. J., M. Curini-Galletti, and E. A. Herniou. 2000. The interrelationships of

733   Proseriata (Platyhelminthes: Seriata) tested with molecules and morphology. Molecular

734   Phylogenetics and Evolution 16:449-466. https://doi.org/10.1006/mpev.2000.0802

735   Long-Fox, B. L. 2022. Phylogenetic controls on shell morphology in the chemosymbiotic

736   Lucinidae (Bivalvia). PhD Dissertation, South Dakota School of Mines and Technology.

737   Mikkelsen, P. M., and R. Bieler. 2008. Seashells of Southern Florida. Living marine molluscs of

738   the Florida Keys and adjacent regions. Bivalves. Princeton University Press, Princeton, 503

739   pp.

740   Oschmann, W. 1993. Environmental oxygen fluctuations and the adaptive response of marine

741   benthic organisms. Journal of the Geological Society 150(1):187-191.

742   https://doi.org/10.1144/gsjgs.150.1.018

743   Paradis, E., and K. Schliep. 2019. ape 5.0: an environment for modern phylogenetics and

744   evolutionary analyses in R. Bioinformatics 35(3):526-528.

745   https://doi.org/10.1093/bioinformatics/bty633

746   Paradis, E., J. Claude, and K. Strimmer. 2004. ape: Analyses of phylogenetics and evolution in R

747   language. Bioinformatics 20(2):289-290. https://doi.org/10.1093/bioinformatics/btg412

748   Polly, D. P., A. M. Lawing, A. Fabre, and A. Goswami. 2013. Phylogenetic principal

749   components analysis and geometric morphometrics. Hystrix the Italian Journal of

750   Mammalogy 24(1):33-41. https://doi.org/10.4404/hystrix-24.1-6383

751   Posada, D. 2008. jModelTest: phylogenetic model averaging. Molecular Biology and Evolution

752   25:1253-1256. https://doi.org/10.1093/molbev/msn083

753   R Core Team. 2020. R: A language and environment for statistical computing.

754   Rambaut, A. 2018. FigTree. http://tree.bio.ed.ac.uk/.

755   Revell, L. J. 2009. Size-correction and principal components for interspecific comparative

756   studies. Evolution 63(12):3258-3268. https://doi.org/10.1111/j.1558-5646.2009.00804.x

757   Rohlf, F. J. 2002. Geometric morphometrics and phylogeny, *in* N. MacLeod, and P. L. Forey,

758   eds., Morphology, shape and phylogeny. CRC Press, Boca Raton, FL. Pp. 175–193.

759   Rohlf, F. J. 2017. tpsDig2. Version 2.31. Department of Ecology and Evolution, State University

760   of New York at Stony Brook. http://life.bio.sunysb.edu/morph/

761   Rohlf, F. J., and D. E. Slice. 1990. Extensions of the Procrustes method for the optimal

762   superimposition of landmarks. Systematic Zoology 39:40-59.

763   Ronquist, F. and J. P. Huelsenbeck. 2003. MRBAYES 3: Bayesian phylogenetic inference under

764   mixed models. Bioinformatics 19:1572-1574. https://doi.org/10.1093/bioinformatics/btg180

765   Sanna, D., T. Lai, P. Cossu, F. Scarpa, G. L. Dedola, B. Cristo, P. Francalacci, M. Curini-

766   Galletti, L. Mura, N. Fois, F. Maltagliati, and M. Casu. 2017. Cytochrome c oxidase subunit I

767   variability in *Ruditapes decussatus* (Veneridae) from the western Mediterranean. The

768   European Zoological Journal 84(1):554-565. https://doi.org/10.1080/24750263.2017.1395914

769   Sayers, E. W., M. Cavanaugh, K. Clark, J. Ostell, K. D. Pruitt, and I. Karsch-Mizrachi. 2020.

770   GenBank. Nucleic Acids Research 48:D84-86. https://doi.org/0.1093/nar/gkz956

771   Sayers, E. W., M. Cavanaugh, K. Clark, K. D. Pruitt, C. L. Schoch, S. T. Sherry, and I. Karsch-

772   Mizrachi. 2021. GenBank. Nucleic Acids Research 49(D1):D92-D96.

773   https://doi.org/10.1093/nar/gkaa1023

774   Schlager, S. 2017. Morpho and Rvcg – Shape Analysis in R: R-Packages for geometric

775   morphometrics, shape analysis and surface manipulations. Methods, Impelementation and

776   Applications 217-246. https://doi.org/10.1016/B978-0-12-810493-4.00011-0

777   Seilacher, A. 1985. Bivalve morphology and function. Series in Geology, Notes for Short Course

778   13:88-101. doi:10.1017/S0271164800001111

779   Shorthouse, D. P. 2010. SimpleMappr, an online tool to produce publication-quality point maps.

780   [Retrieved from https://www.simplemappr.net. Accessed August 2021].

781   Sidlauskas, B. L. 2008. Continuous and arrested morphological diversification in sister clades of

782   characiform fishes: a phylomorphospace approach. Evolution 62:3135–3156.

783   https://doi.org/10.1111/j.1558-5646.2008.00519.x

784   Stanley, S. M. 1970. Relation of shell form to life habits of the Bivalvia (Mollusca). Geological

785   Society of America Memoir, 125, 1-296.

786   Stanley, S. M. 1988. Adaptive Morphology of the Shell in Bivalves and Gastropods. The

787   Mollusca 11:105-141.

788   Stanley, S. M. 2014. Evolutionary radiation of shallow-water Lucinidae (Bivalvia with

789   endosymbionts) as a result of the rise of seagrasses and mangroves. Geology 42:803-806.

790   https://doi.org/10.1130/G35942.1

791   Stayton, C. T. 2015. The definition, recognition, and interpretation of convergent evolution, and

792   two new measures for quantifying and assessing the significance of convergence. Evolution

793   69(8):2140-2153. https://doi.org/10.1111/evo.12729

794   Talavera, G., and J. Castresana. 2007. Improvement of phylogenies after removing divergent and

795   ambiguously aligned blocks from protein sequence alignments. Systematic Biology

796   56(4):564-577. https://doi.org/10.1080/10635150701472164

797   Tarnowska, K. A. Chenuil, R. Nikula, J. P. Feral, and M. Wolowicz. 2010. Complex genetic

798   population structure of the bivalve *Cerastoderma glaucum* in a highly fragmented lagoon

799   habitat. Marine Ecology Progress Series 406:173-184. https://doi.org/10.3354/meps08549

800   Taylor, J. D., and E. A. Glover. 2000. Functional anatomy, chemosymbiosis and evolution of the

801   Lucinidae, *in* E. M. Harper, J. D. Taylor, and J. A. Crame, eds., The Evolutionary Biology of

802   the Bivalvia, Geological Society of London Special Publication, 177:207–225.

803   https://doi.org/10.1144/GSL.SP.2000.177.01.12

804   Taylor, J. D., and E. A. Glover. 2006. Lucinidae – the most diverse group of chemosymbiotic

805   molluscs. Zoological Journal of the Linnean Society 148:421–438.

806   https://doi.org/10.1111/j.1096-3642.2006.00261.x

807   Taylor, J. D., and E. A. Glover. 2010. Chemosymbiotic Bivalves, *in* S. Kiel, ed., The Vent and

808   Seep Biota. Topics in Geobiology, vol 33. Springer, Dordrecht. https://doi.org/10.1007/978-

809   90-481-9572-5_5

810   Taylor, J. D., E. A. Glover, and S. T. Williams. 2008. Ancient chemosynthetic bivalves:

811   systematics of Solemyidae from eastern and southern Australia (Mollusca: Bivalvia), *in* P. J.

812   F. Davie, and J. A. Phillips, eds., Proceedings of the Thirteenth International Marine

813   Biological Workshop, The Marine Fauna and Flora of Moreton Bay, Queensland. Memoirs of

814   the Queensland Museum - Nature 54:75-104.

815   Taylor, J. D., E. A. Glover, L. Smith, P. Dyal, and S. T. Williams. 2011. Molecular phylogeny

816   and classification of the chemosymbiotic bivalve family Lucinidae (Mollusca: Bivalvia).

817   Zoological Journal of the Linnean Society 163:15-49. https://doi.org/10.1111/j.1096-

818   3642.2011.00700.x

819   Taylor, J. D., E. A. Glover, and S. T. Williams. 2013. Taxonomy and phylogeny of western

820   Atlantic Lucinidae: new genus for *Lucina costata* d'Orbigny, 1846, a new species of

821   *Ferrocina* and neotype designation for *Venus orbiculata* (Montagu, 1808). The Nautilus

822   127:131-146.

823   Taylor, J. D., E. A. Glover, and S. T. Williams. 2014. Diversification of chemosymbiotic

824   bivalves: origins and relationships of deeper water Lucinidae. Biological Journal of the

825   Linnean Society 111:401-420. https://doi.org/10.1111/bij.12208

826   Taylor, J. D., E. A. Glover, L. Smith, C. Ikebe, and S. T. Williams. 2016. New molecular

827   phylogeny of Lucinidae: Increased taxon base with focus on tropical Western Atlantic species

828   (Mollusca: Bivalvia). Zootaxa 4196(3):381-398. https://doi.org/10.11646/zootaxa.4196.3.2

829   Tomašových, A., I. Gallmetzer, A. Haselmair, D. S. Kaufman, M. Kralj, D. Cassin, R. Zonta,

830   and M. Zuschin. 2018. Tracing the effects of eutrophication on molluscan communities in

831   sediment cores: outbreaks of an opportunistic species coincide with reduced bioturbation and

832   high frequency of hypoxia in the Adriatic Sea. Paleobiology 44(4):575-602.

833   https://doi.org/10.1017/pab.2018.22

834   Uyeda, J. C., D. S. Caetano, and M. W. Pennell. 2015. Comparative analysis of principal

835   components can be misleading. Systematic Biology 64(4)677-689.

836   https://doi.org/10.1093/sysbio/syv019

837   Williams, S. T., D. G. Reid, and D. T. J. Littlewood. 2003. A molecular phylogeny of the

838   Littorininae (Gastropoda: Littorinidae): unequal evolutionary rates, morphological

839   parallelism, and biogeography of the Southern Ocean. Molecular Phylogenetics and Evolution

840   28:60-86. https://doi.org/10.1016/S1055-7903(03)00038-1

841   Williams, S. T., J. D. Taylor, and E. A. Glover. 2004. Molecular phylogeny of the Lucinoidea

842   (Bivalvia): non-monophyly and separate acquisition of bacterial chemosymbiosis. Journal of

843   Molluscan Studies 70:187-202. https://doi.org/10.1093/mollus/70.2.187

844   Winnepenninckx, B. M. H., D. G. Reid, and T. Backeljau. 1998. Performance of 18S rRNA in

845   littorinid phylogeny (Gastropoda: Caenogastropoda). Journal of Molecular Evolution 47:586-

846   596. https://doi.org/10.1007/pl00006415

847   Zanatta, D. T., and R. W. Murphy. 2008. The phylogeographical and management implications

848   of genetic population structure in the imperiled snuffbox mussel, *Epioblasma triquetra*

849   (Bivalvia: Unionidae). Biological Journal of the Linnean Society 93(2):371-384.

850   https://doi.org/10.1111/j.1095-8312.2007.00936.x

851   Zelditch, M. L., D. L. Swiderski, and H. D. Sheets. 2012. Geometric morphometrics for

852   biologists: a primer. Academic Press, London.

853